medium supplemented with 10% fetal bovine serum (Wisent, Rocklin, CA), 100 units/ml penicillin/streptomycin, and 2 mM L-glutamine (Invitrogen). Transient transfections were performed in six-well dishes using the polyethylenimine (Polysciences, Warrington, PA) method.

Plasmids—CXCR4-YFP and CXCR7-YFP have been described previously (3). Plasmids encoding β-arrestin 2-Rluc (a generous gift of Michel Bouvier) have been described previously (15). To generate the C-terminal chimers, a unique BsiWI restriction site was inserted in CXCR4-YFP and CXCR7-YFP using the QuikChange Multi site-directed mutagenesis kit (Stratagene), according to the manufacturer's instructions. The C-terminal domains were excised by BsiWI/NotI digestion and ligated into the respective opposite plasmid. The BsiWI site was then removed by site-directed mutagenesis, restoring the respective CXCR7 and CXCR4 sequences. The primers used for the site-directed mutagenesis were: CXCR4-mut916-BsiWI, 5′-CATCCTCTATGCTTTCCTCGTACGCAAATTTAAAACCTCTGCC-3′; CXCR7-mut955-BsiWI, 5′-CCCTGTCCTCTACAGCTTCATCGTACGCAACTACAGGTACGAGC-3′; CXCR4-X7Cter-WT, 5′-CATCCTCTATGCTTTCCTTAATCGCAACTACAGGTACGAGC-3′; CXCR7-X4Cter-WT, 5′-CCCTGTCCTCTACAGCTTCATCGGAGCCAAATTTAAAACCTCTGCCC-3′.

Radioligand Binding Assays—Cell membrane preparation and binding assays were performed as described previously (16) with minor modifications. Briefly, HEK293E cells expressing the respective receptor were washed once with PBS and subjected to one freeze-thaw cycle. Broken cells were then gently scraped in resuspension buffer (50 mM Hepes, pH 7.4, 1 mM $CaCl_2$, and 5 mM $MgCl_2$), centrifuged at 3500 × *g* for 15 min at 4 °C, and resuspended in binding buffer (50 mM Hepes, pH 7.4, 1 mM $CaCl_2$ 5 mM $MgCl_2$, 140 mM NaCl, 0.5% BSA). For competition binding assays, broken cells (1 μg of protein) were incubated for 1 h at room temperature in binding buffer with 0.03 nM [^{125}I]-SDF-1α as a tracer and increasing concentrations of competitor. Bound radioactivity was separated from free ligand by filtration, and receptor-bound radioactivity was quantified by γ-radiation counting.

BRET Measurements—β-Arrestin recruitment was measured by BRET essentially as described previously (17). HEK293T cells were cotransfected with 1 μg of receptor-eYFP construct with 0.05 μg of β-arrestin 2-Rluc. For [acceptor]/[donor] titrations, 0.05 μg of β-arrestin 2-Rluc was cotransfected with increasing amounts of the receptor-eYFP construct. All transfections were completed to 2 μg/well with empty vector. Following overnight culture, transiently transfected HEK293 cells were seeded in 96-well, white, clear bottom microplates (ViewPlate; PerkinElmer Life Sciences) coated with poly(D-lysine) and left in culture for 24 h. Cells were washed once with PBS, and the Rluc substrate coelenterazine h (NanoLight Technology, Pinetop, AZ) was added at a final concentration of 5 μM to BRET buffer (PBS, 0.5 mM $MgCl_2$, 0.1% glucose). BRET readings were collected using a Mithras LB940 plate reader (Berthold Technologies, Bad Wildbad, Germany) and MicroWin2000 software. BRET measurement between Rluc and YFP was obtained by sequential integration of the signals in the 460–500 nm (Rluc) and 510–550 nm (YFP) windows. The BRET signal was calculated as the ratio of light emitted by acceptor (YFP) over the light emitted by donor (Rluc). The values were corrected to net BRET by subtracting the background BRET signal obtained in cells transfected with the Rluc construct alone. β-Arrestin recruitment was measured 30 min after ligand addition.

Flow Cytometric Analysis—Receptor cell surface expression was confirmed by flow cytometry using anti-CXCR7-APC (clone 358426) and anti-CXCR4-APC (clone 12G5, both from R&D Systems). Cells were washed three times in ice-cold PBS, resuspended, and stained with antibody for 30 min at 4 °C. After a final wash, the cells were resuspended in 0.5% paraformaldehyde and analyzed using a FACSCalibur Flow Cytometer (BD Biosciences).

Data Analysis—Data from BRET assays were the mean of independent experiments, each of which was performed in triplicate. Curve fitting by nonlinear regression and statistical analysis was conducted using GraphPad Prism 4 software (GraphPad Software Inc., San Diego, CA). Statistical significance of the differences between more than two groups was calculated by one-way analysis of variance followed by Tukey's post test.

RESULTS

β-Arrestin Recruitment to CXCR7 by TC14012—We previously found that a small molecule antagonist of CXCR4, AMD3100, acted as an agonist on CXCR7 in that it induced recruitment of β-arrestin 2 to the receptor, albeit with low potency. Based on this finding, we tested whether this property was shared by different CXCR4 inhibitors. We thus tested the ability of TC14012, a serum-stable derivative of the peptidomimetic T140, to induce recruitment of β-arrestin 2 to CXCR7, using a previously reported BRET-based experimental system (17). As shown in Fig. 1*A*, TC14012 was found to be a potent and efficient agonist of β-arrestin recruitment to CXCR7, with an apparent EC_{50} of 350 nM. This is almost 3 logs more potent than AMD3100 (EC_{50} of 138 μM) and approximately one log less potent than the efficiency of the cognate CXCR7 chemokine ligand CXCL12 in this system (30 nM). The EC_{50} is in line with the IC_{50} of TC14012 observed in radioligand displacement assays using HEK293 cells stably expressing CXCR7 and radiolabeled CXCL12 (K_i of 157 nM ± 36, $n = 3$, data not shown). These experiments show that the previously reported capacity of AMD3100 to recruit β-arrestin to CXCR7 is shared by a second, structurally unrelated CXCR4 antagonist. To further confirm signaling downstream of arrestin (4), we addressed Erk phosphorylation by TC14012 via CXCR7 in untransfected U373 glioma cells that express endogenous CXCR7 but no CXCR4, unlike HEK293 cells that express trace amounts of both receptors. TC14012, like CXCL12, leads to sustained Erk 1/2 phosphorylation in these cells (supplemental methods and Fig. S1).

Design and Expression of CXCR4-CXCR7 Chimeras—Although limited receptor selectivity of synthetic chemokine receptor ligands is not uncommon, we were intrigued by the finding that both shared ligands of CXCR4 and CXCR7 had antagonistic activity on CXCR4, whereas they agonistically induced β-arrestin recruitment to CXCR7. Our interpretation

is that these divergent effects are not fortuitous but rather indicate differences between the two receptors in the activation mechanism of β-arrestin recruitment. Such differences might be due to differences in regulatory determinants for the recruitment of arrestin encoded by the receptor C termini. Alternatively, differences between the CXCR4 and CXCR7 cores could entail different ligand-induced receptor rearrangements that translate into inhibition of arrestin recruitment in one case but activation in the other.

To address this issue, we constructed chimeric CXCR4-CXCR7 receptors by exchanging the C-terminal domains of one receptor onto the other (named CXCR4-Cter7 and CXCR7-Cter4, supplemental Fig. S2*A*). All constructs were expressed at the cell surface and detected by respective monoclonal antibodies by flow cytometry (supplemental Fig. S2*B*).

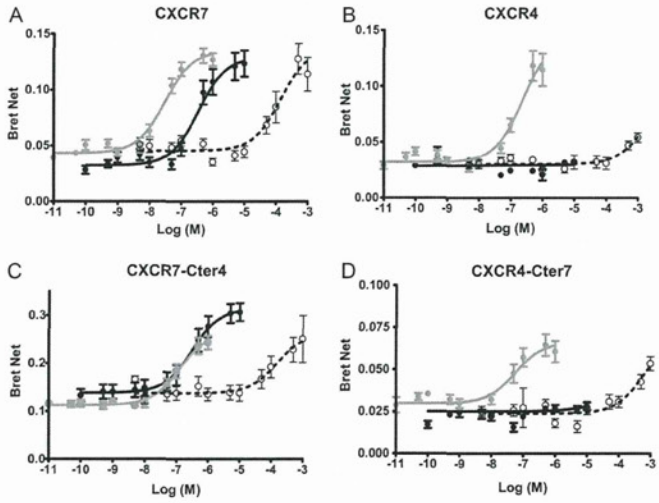

FIGURE 1. **Effect of natural and synthetic ligands on the β-arrestin recruitment to CXCR4, CXCR7, and receptor chimeras.** HEK293 cells transiently coexpressing β-arrestin 2-RLuc as a BRET donor and respective receptors fused to the BRET acceptor YFP were stimulated with the indicated concentrations of CXCL12 (*gray circles*), TC14012 (*black circles*), or AMD3100 (*open circles*). Resulting BRET measurements are given as $BRET_{net}$. Data are mean values from 5–9 (CXCL12) or 3–7 (TC14012 and AMD3100) independent experiments, each performed in triplicate. *Error bars* indicate S.E. For statistical analysis, see Table 1. *A*, CXCR7; *B*, CXCR4; *C*, CXCR7-Cter4; *D*, CXCR4-Cter4.

β-Arrestin Recruitment to Chimeric Receptors Induced by Natural and Synthetic Ligands—Using the respective receptors/chimeras, we then tested β-arrestin recruitment induced by the different ligands in dose-response experiments (Fig. 1 and Table 1). Significantly higher BRET was observed with the CXCR7-Cter4 chimera in the absence of ligand, suggesting constitutive recruitment of arrestin by this chimera. Upon stimulation with TC14012, CXCR7 and the CXCR7-Cter4 chimera were able to recruit arrestin, whereas CXCR4 and CXCR4-Cter7 remained silent. A similar pattern was observed with AMD3100. These data show that it is the core of CXCR7, and not its C terminus, that is responsible for the CXCR7 response to the synthetic ligands.

The use of quantitative BRET permitted additional observations concerning the respective responses to CXCL12. The responses of CXCR7 and the CXCR4-Cter7 chimera were significantly more potent (EC_{50} of 30 and 58 nM, respectively) than those of CXCR4 and the CXCR7-Cter4 chimera (EC_{50} of 242 and 191 nM, respectively) (CXCR4 *versus* CXCR7, $p < 0.01$; CXCR4 *versus* CXCR4-Cter7 and CXCR7 *versus* CXCR7-Cter4, $p < 0.05$; see also Table 1). This suggests that unlike the ability to respond to TC14012, the potency of the response to CXCL12 was determined by the respective C termini, possibly reflecting their effectiveness in translating ligand-induced conformational changes into arrestin recruitment. We cannot formally exclude the possibility that this was due to the C-terminal YFP BRET-fusion that might affect the regulatory function of this domain. However, our observation that the potency of arrestin recruitment to CXCR7 was identical in an alternative BRET system with unfused CXCR7 and a dual brilliance Rluc-arrestin-YFP fusion (18) (data not shown) speaks against a role of the fusion for potency and supports the idea that the receptor C terminus indeed determines the potency of the arrestin response.

Spontaneous Arrestin Recruitment to CXCR7-Cter4 in Absence of Ligand—To further evaluate the constitutive BRET signal yielded by the CXCR7-Cter4 chimera, we performed

TABLE 1

Curve-fitting parameters of arrestin recruitment to CXCR4, CXCR7, and the respective chimeras

The table summarizes the curve parameters of the activation of arrestin recruitment to the different receptors and chimera by CXCL12, TC14012, and AMD3100 shown in Fig. 1. The differences in EC_{50} upon stimulation with CXCL12 were statistically significant between CXCR4 and CXCR7 ($p < 0.001$); CXCR4 and CXCR4-Cter7 ($p < 0.05$); and CXCR7 and CXCR7-Cter4 ($p < 0.01$) (one-way analysis of variance with Tukey's post test). The difference of the curve bottom between CXCR7-Cter4 and all other receptors was also significant ($p < 0.001$). The difference of the curve bottom between CXCR7 and CXCR4 was not statistically significant. The very high EC_{50} values observed for AMD3100 (1.5 and 0.5 mM) on CXCR4 and CXCR4-Cter7 may reflect experimental artifacts at extreme doses of the compound (higher than those applied in our previous report (3)). Alternatively, they may represent weak agonist activity of AMD3100 also on CXCR4, in line with its previous description as a partial agonist (11, 19). NA, not applicable.

	CXCL12					TC14012					AMD3100				
receptor	EC_{50} (nM)	$logEC_{50}$± SEM	top	bottom	n	EC_{50} (nM)	$logEC_{50}$± SEM	top	bottom	n	EC_{50} (μM)	$logEC_{50}$± SEM	top	bottom	n
CXCR4	242	-6,62±0,17	0,14±0,01	0,03±0,00	6	N/A	N/A	N/A	N/A	3	1629	-2,79±0,98	0,09±0,11	0,03±0,00	3
CXCR7	30	-7,52±0,09	0,13±0,00	0,04±0,00	9	350	-6,46±0,14	0,13±0,01	0,03±0,00	7	138	-3,86±0,19	0,14±0,01	0,05±0,00	3
CXCR4-CtailX7	56	-7,25±0,21	0,07±0,00	0,03±0,00	5	N/A	N/A	N/A	N/A	3	570	-3,24±0,55	0,07±0,03	0,03±0,00	3
CXCR7-CtailX4	191	-6,90±0.14	0,27±0,01	0,11±0,00	6	313	-6,51±0,17	0,31±0,01	0,14±0,01	3	154	-3,81±0,34	0,26±0,03	0,14±0,01	3

BRET acceptor/donor titrations in the absence and presence of 100 nM CXCL12. In the absence of chemokine, CXCR7-YFP titrations over β-arrestin 2-Rluc yielded a straight line representing increasing nonspecific bystander BRET (19), in line with the absence of baseline arrestin recruitment (supplemental Fig. S3). However, the CXCR7-Cter4 chimera yielded a saturable hyperbolic curve, in line with specific BRET resulting from spontaneous arrestin recruitment by this chimera. In curve-fitting analysis, the preferred model for the curve yielded by CXCR7-Cter4 in the absence of ligand was consistently hyperbolic ($p < 0.001$, $n = 4$), unlike for CXCR7, where the preferred model in the absence of ligand was a straight line. In the presence of 100 nM CXCL12, [acceptor]/[donor] titrations of both receptors yielded specific BRET as hyperbolic curves. The $BRET_{50}$ is a measure of the propensity with which an interaction takes place (19). Remarkably, in simultaneous curve fittings, the $BRET_{50}$ of the CXCR7-Cter4 mutant is significantly smaller in the presence of the chemokine than in its absence ($p < 0.001$ in 3 out of 4 experiments, and $p < 0.01$ in one 1 out of 4 experiments). This indicates that the constitutive activity of the CXCR7-Cter4 chimera is further activated by the presence of CXCL12.

DISCUSSION

The main finding of the present report is that the polyphemusin derivative TC14012, a CXCR4 inverse agonist (11, 12), also binds CXCR7 but acts here as an agonist of the arrestin pathway. Although this is similar to the previously reported agonist activity on CXCR7 of the structurally unrelated CXCR4 inhibitor AMD3100, TC14012 is a much more potent agonist on CXCR7 (EC_{50} of 350 nM for TC14012 *versus* 140 μM for AMD3100) and only one log weaker than the natural chemokine agonist CXCL12 (35 nM). Given that AMD3100 and TC14012 are structurally unrelated and that both receptors also share a natural ligand, we envision that the cross-reactivity of both synthetic ligands results from structural similarities of the ligand-binding surfaces of CXCR4 and CXCR7.

Lack of selectivity for one given chemokine receptor of synthetic ligands has hampered the development of drug candidates targeting chemokine receptors, and our results suggest that newly developed CXCR4 inhibitors should also be routinely tested on CXCR7. However, previous work with different T140 analogues (20) and the recent findings that the small molecule FC131 does not bind to CXCR7 (21) and does not induce arrestin recruitment to CXCR7 [5] indicate that CXCR4 inhibitors do not inherently also bind CXCR7 and that receptor selectivity can be achieved. To our knowledge, synthetic chemokine receptor ligands that exert opposite effects on two different receptors are still unreported. Of note, receptor promiscuity being a hallmark of natural chemokine receptor ligands, such inverse action on different receptors also exists among natural chemokine receptor ligands, but the structural basis for these opposite effects remains yet unknown. Although nonselectivity of synthetic 7TMR ligands is generally seen as a drawback in drug development, simultaneous agonism on one receptor and antagonism on a second one might actually be of advantage in specific settings. This emerging concept especially applies to 7TMRs that functionally and/or physically interact and that share endogenous ligands. For example, simultaneous activation of the μ-opioid receptor and inhibition of the δ-opioid receptor are desired properties that have been shown to positively alter the side-effect profile (tolerance and dependence) of analgesics such as morphine, which activates both the μ-opioid receptor and the δ-opioid receptor (22). In this context, the documented physical and functional interactions between CXCR4 and CXCR7 (5, 7, 8) should be kept in mind. CXCR4 inhibition interferes with cancer biology at multiple steps including cancer cell growth and dissemination. Moreover, synthetic ligands of CXCR7, CCX451, CCX754, and CCX771 also reduce tumor growth and transendothelial migration (2, 6). Interestingly, rather than being a CXCR7 inhibitor, at least CCX771 turned out to be a potent activator of arrestin recruitment to CXCR7 (6). Taken together, these data suggest that simultaneous inhibition of CXCR4 and activation of CXCR7 might indeed be of interest in the context of cancer treatment.

The results obtained with CXCR4-CXCR7 C terminus-swapping chimera identified the receptor core as the determinant for the agonistic activity of TC14012 and AMD3100 on CXCR7. This finding was unexpected insofar as that for both CXCR4 and CXCR7, the C terminus is a crucial arrestin recruitment determinant. Phosphorylation of C-terminal serine residues promotes β-arrestin 2 recruitment to CXCR4 (14), and deletion of 43 CXCR7 C-terminal residues results in loss of arrestin recruitment (6). Our finding that the potency of arrestin recruitment in response to CXCL12 depends on the receptor C terminus is in line with a regulatory role of this domain. Although independence of arrestin recruitment from receptor phosphorylation (but still dependence on the receptor C terminus) has been described for some 7TMRs, among which is the chemokine scavenger receptor D6, which constitutively recruits β-arrestin (23), we find that CXCR7, which has also been suggested to be a chemokine scavenger receptor (24, 25), does not constitutively recruit β-arrestin. In this context, our finding that the CXCR7-Cter4 chimera associates with β-arrestin in the absence of ligand is intriguing and might reflect the overall greater proclivity of CXCR7 to recruit arrestin.

The opposite effects of TC14012 and AMD3100 on CXCR4 and CXCR7 thus reflect differences between their respective activation mechanisms of the arrestin pathway that are located in the receptor core. Despite growing information about interactions that contribute to binding of chemokines to their receptors (mostly involving the structured chemokine core and the receptor N terminus), the chemokine receptor determinants for activation still remain elusive. Similar to other studied chemokine-receptor couples, CXCR4 activation requires the flexible N terminus of CXCL12, and in particular, the lysine and proline residues in positions 1 and 2 (26). However, to date, and because of the lacking identification of receptor residues that are directly involved in interactions with the chemokine N terminus, only speculative models of chemokine receptor activation have been forwarded. This

[5] S. Gravel and N. Heveker, unpublished data.

remains true despite the recent publication of the CXCR4 crystal structure in the presence of small antagonists (27) (PDB codes 3ODU, 3OE0, 3OE9, and 3OE6). With reference to earlier models (26), a recent report puts forward the hypothesis that insertion of the CXCL12 N terminus into the cavity formed by the CXCR4 transmembrane helices was required for activation, similar to binding pockets for small agonists of other class A 7TMRs (28). This is supported by data that show that AMD3100 prevents interaction of the CXCL12 N terminus with this cavity but not other receptor-chemokine interactions (28).

Following this model, our results indicate that CXCR7 activation does not require the CXCL12 N terminus interaction in the same way as does CXCR4 because activation by the chemokine is not blocked by the small molecule ligands. Rather, CXCR7 activation determinants actually overlap with the AMD3100-CXCR7 and TC14012-CXCR7 interaction determinants because both ligands promote CXCR7 activation. Intriguingly, with CXCR4, the interactions of both compounds have been mapped to the transmembrane domain/extracellular loop intersection rather than to the depth of the transmembrane crevice (11, 29, 30). At least for AMD3100, a similar binding mode to both CXCR4 and CXCR7 can be inferred by the conservation of CXCR4 key residues Asp-171 and Asp-262 for AMD3100 interaction in CXCR7. It is thus tempting to speculate that CXCR7 activation determinants are rather close to the surface, whereas those of CXCR4 are located deeper in the crevice of the receptor. More work about the respective activation mechanisms of CXCR4 and CXCR7 by CXCL12 will be needed to test this hypothesis.

Acknowledgments—We are indebted to Geneviève Saint-Onge, Marie-Ève Pelletier, and Guillaume Sylvian-Drolet for expert technical assistance.

REFERENCES

1. Balabanian, K., Lagane, B., Infantino, S., Chow, K. Y., Harriague, J., Moepps, B., Arenzana-Seisdedos, F., Thelen, M., and Bachelerie, F. (2005) *J. Biol. Chem.* **280,** 35760–35766
2. Burns, J. M., Summers, B. C., Wang, Y., Melikian, A., Berahovich, R., Miao, Z., Penfold, M. E., Sunshine, M. J., Littman, D. R., Kuo, C. J., Wei, K., McMaster, B. E., Wright, K., Howard, M. C., and Schall, T. J. (2006) *J. Exp. Med.* **203,** 2201–2213
3. Kalatskaya, I., Berchiche, Y. A., Gravel, S., Limberg, B. J., Rosenbaum, J. S., and Heveker, N. (2009) *Mol. Pharmacol.* **75,** 1240–1247
4. Rajagopal, S., Kim, J., Ahn, S., Craig, S., Lam, C. M., Gerard, N. P., Gerard, C., and Lefkowitz, R. J. (2010) *Proc. Natl. Acad. Sci. U.S.A.* **107,** 628–632
5. Hartmann, T. N., Grabovsky, V., Pasvolsky, R., Shulman, Z., Buss, E. C., Spiegel, A., Nagler, A., Lapidot, T., Thelen, M., and Alon, R. (2008) *J. Leukoc Biol.* **84,** 1130–1140
6. Zabel, B. A., Wang, Y., Lewén, S., Berahovich, R. D., Penfold, M. E., Zhang, P., Powers, J., Summers, B. C., Miao, Z., Zhao, B., Jalili, A., Janowska-Wieczorek, A., Jaen, J. C., and Schall, T. J. (2009) *J. Immunol.* **183,** 3204–3211
7. Sierro, F., Biben, C., Martínez-Muñoz, L., Mellado, M., Ransohoff, R. M., Li, M., Woehl, B., Leung, H., Groom, J., Batten, M., Harvey, R. P., Martínez-A., C., Mackay, C. R., and Mackay, F. (2007) *Proc. Natl. Acad. Sci. U.S.A.* **104,** 14759–14764
8. Levoye, A., Balabanian, K., Baleux, F., Bachelerie, F., and Lagane, B. (2009) *Blood* **113,** 6085–6093
9. Thelen, M., and Thelen, S. (2008) *J. Neuroimmunol.* **198,** 9–13
10. Tamamura, H., Xu, Y., Hattori, T., Zhang, X., Arakaki, R., Kanbara, K., Omagari, A., Otaka, A., Ibuka, T., Yamamoto, N., Nakashima, H., and Fujii, N. (1998) *Biochem. Biophys. Res. Commun.* **253,** 877–882
11. Trent, J. O., Wang, Z. X., Murray, J. L., Shao, W., Tamamura, H., Fujii, N., and Peiper, S. C. (2003) *J. Biol. Chem.* **278,** 47136–47144
12. Zhang, W. B., Navenot, J. M., Haribabu, B., Tamamura, H., Hiramatu, K., Omagari, A., Pei, G., Manfredi, J. P., Fujii, N., Broach, J. R., and Peiper, S. C. (2002) *J. Biol. Chem.* **277,** 24515–24521
13. Tamamura, H., Omagari, A., Hiramatsu, K., Gotoh, K., Kanamoto, T., Xu, Y., Kodama, E., Matsuoka, M., Hattori, T., Yamamoto, N., Nakashima, H., Otaka, A., and Fujii, N. (2001) *Bioorg Med. Chem. Lett.* **11,** 1897–1902
14. Busillo, J. M., Armando, S., Sengupta, R., Meucci, O., Bouvier, M., and Benovic, J. L. (2010) *J. Biol. Chem.* **285,** 7805–7817
15. Perroy, J., Adam, L., Qanbar, R., Chénier, S., and Bouvier, M. (2003) *EMBO J.* **22,** 3816–3824
16. Boulais, P. E., Dulude, D., Cabana, J., Heveker, N., Escher, E., Lavigne, P., and Leduc, R. (2009) *Biochem. Pharmacol.* **78,** 1382–1390
17. Hamdan, F. F., Audet, M., Garneau, P., Pelletier, J., and Bouvier, M. (2005) *J. Biomol. Screen.* **10,** 463–475
18. Charest, P. G., Terrillon, S., and Bouvier, M. (2005) *EMBO Rep.* **6,** 334–340
19. Mercier, J. F., Salahpour, A., Angers, S., Breit, A., and Bouvier, M. (2002) *J. Biol. Chem.* **277,** 44925–44931
20. Oishi, S., Masuda, R., Evans, B., Ueda, S., Goto, Y., Ohno, H., Hirasawa, A., Tsujimoto, G., Wang, Z., Peiper, S. C., Naito, T., Kodama, E., Matsuoka, M., and Fujii, N. (2008) *Chembiochem* **9,** 1154–1158
21. Narumi, T., Hayashi, R., Tomita, K., Kobayashi, K., Tanahara, N., Ohno, H., Naito, T., Kodama, E., Matsuoka, M., Oishi, S., and Fujii, N. (2010) *Org Biomol Chem.* **8,** 616–621
22. Schiller, P. W. (2010) *Life Sci.* **86,** 598–603
23. Galliera, E., Jala, V. R., Trent, J. O., Bonecchi, R., Signorelli, P., Lefkowitz, R. J., Mantovani, A., Locati, M., and Haribabu, B. (2004) *J. Biol. Chem.* **279,** 25590–25597
24. Boldajipour, B., Mahabaleshwar, H., Kardash, E., Reichman-Fried, M., Blaser, H., Minina, S., Wilson, D., Xu, Q., and Raz, E. (2008) *Cell* **132,** 463–473
25. Naumann, U., Cameroni, E., Pruenster, M., Mahabaleshwar, H., Raz, E., Zerwes, H. G., Rot, A., and Thelen, M. (2010) *PLoS One* **5,** e9175
26. Crump, M. P., Gong, J. H., Loetscher, P., Rajarathnam, K., Amara, A., Arenzana-Seisdedos, F., Virelizier, J. L., Baggiolini, M., Sykes, B. D., and Clark-Lewis, I. (1997) *EMBO J.* **16,** 6996–7007
27. Wu, B., Chien, E. Y. T., Mol, C. D., Fenalti, G., Liu, W., Katritch, V., Abagyan, R., Brooun, A., Wells, P., Bi, F. C., Hamel, D. J., Kuhn, P., Handel, T. M., Cherzov, V., and Stevens, R. C. (2010) *Science*, in press
28. Kofuku, Y., Yoshiura, C., Ueda, T., Terasawa, H., Hirai, T., Tominaga, S., Hirose, M., Maeda, Y., Takahashi, H., Terashima, Y., Matsushima, K., and Shimada, I. (2009) *J. Biol. Chem.* **284,** 35240–35250
29. Labrosse, B., Brelot, A., Heveker, N., Sol, N., Schols, D., De Clercq, E., and Alizon, M. (1998) *J. Virol.* **72,** 6381–6388
30. Gerlach, L. O., Skerlj, R. T., Bridger, G. J., and Schwartz, T. W. (2001) *J. Biol. Chem.* **276,** 14153–14160

CXCL12-CXCR4 chemokine signaling is essential for NK-cell development in adult mice

Mamiko Noda,[1] Yoshiki Omatsu,[1] Tatsuki Sugiyama,[1] Shinya Oishi,[2] Nobutaka Fujii,[2] and Takashi Nagasawa[1]

[1]Department of Immunobiology and Hematology, Institute for Frontier Medical Sciences, and [2]Graduate School of Pharmaceutical Sciences, Kyoto University, Kyoto, Japan

Natural killer (NK) cells are granular lymphocytes that are generated from hematopoietic stem cells and play vital roles in the innate immune response against tumors and viral infection. Generation of NK cells is known to require several cytokines, including interleukin-15 (IL-15) and Fms-like tyrosine kinase 3 ligand, but not IL-2 or IL-7. Here we investigated the in vivo role of CXC chemokine ligand-12 (CXCL12) and its primary receptor CXCR4 in NK-cell development. The numbers of NK cells appeared normal in embryos lacking CXCL12 or CXCR4; however, the numbers of functional NK cells were severely reduced in the bone marrow, spleen, and peripheral blood from adult CXCR4 conditionally deficient mice compared with control animals, probably resulting from cell-intrinsic CXCR4 deficiency. In culture, CXCL12 enhanced the generation of NK cells from lymphoid-primed multipotent progenitors and immature NK cells. In the bone marrow, expression of IL-15 mRNA was considerably higher in CXCL12-abundant reticular (CAR) cells than in other marrow cells, and most NK cells were in contact with the processes of CAR cells. Thus, CXCL12-CXCR4 chemokine signaling is essential for NK-cell development in adults, and CAR cells might function as a niche for NK cells in bone marrow. (*Blood.* 2011;117(2):451-458)

Introduction

Natural killer (NK) cells are large, granular lymphocytes that have an important role in innate immune response against tumors, viral infection, and graft rejection.[1,2] They also elicit adaptive immune responses by producing cytokines, such as interferon-γ (IFN-γ), tumor-necrosis factor-α, and granulocyte-macrophage colony-stimulating factor and chemokines, such as CC chemokine ligand-3 (CCL3), CCL4, and CCL5, as proinflammatory mediators.[2]

NK cells are generated from hematopoietic stem cells (HSCs) in the fetal liver and adult bone marrow. Bipotent T-cell and NK-cell progenitors (p-T/NKs) have been identified in the fetal liver[3] and fetal thymus,[4,5] and the earliest committed NK-cell precursors (NKPs), which are characterized by the expression of CD122 (interleukin-2 receptorβ [IL-2Rβ]),[5] and mature NK cells (mNKs), which express NK-cell markers NK1.1 and DX5,[6] have been detected in the fetal thymus. In adult mice, HSCs give rise to lymphoid-primed multipotent progenitors (LMPPs)[7] and common lymphoid progenitors (CLPs),[8,9] which have the potential to generate NK cells as well as T, B, and dendritic cells (DCs). As in the fetal thymus, $Lin^-NK1.1^-DX5^-CD122^+$ cells have been reported to be the earliest committed NKPs in the marrow.[10] The development of NKPs to immature NK cells (iNKs) is accompanied by the expression of NK1.1, and developing iNKs acquire the expressions of DX5, Mac-1, and Ly49 receptors, including inhibitory or activating NK cell receptors, in an orderly fashion and differentiate into mNKs.[2,11]

Generation of NK cells is regulated by several cytokines produced by microenvironments in the fetal liver and/or bone marrow. In mice lacking IL-15 or its receptors, including IL-15 receptor α (IL-15Rα), IL-2Rβ, and IL-2Rγ, the numbers of NKPs are relatively normal, but the number and cytotoxic activity of NK cells are severely reduced compared with control animals.[12-15] In addition, Fms-like tyrosine kinase 3 ligand (Flt3L)–deficient mice have a reduction in the number and cytotoxic activity of NK cells in the bone marrow.[16] In contrast, IL-2 or IL-7 has been shown to be dispensable for NK-cell development because the numbers of NK cells are normal in mice lacking IL-2,[17,18] IL-7,[18,19] or IL-7Rα.[20] The role of stem cell factor (SCF) and its receptor c-kit in NK-cell development remains a controversial issue. Although viable W/W mice lacking c-kit, termed Vickid mice, show normal NK-cell development,[21] chimeric mice reconstituted with fetal liver cells from W/W mice had a reduction in the number and function of NK cells.[22]

CXC chemokine ligand-12 (CXCL12; also known as stromal cell–derived factor-1 and pre-B-cell-growth-stimulating factor) is a member of the chemokines, a large family of structurally related chemoattractive cytokines, and its primary physiologic receptor is CXCR4, a hepta-helical receptor coupled to heterotrimeric G proteins, which also functions as an entry receptor for HIV-1.[23] Previous studies using mice lacking CXCL12 or CXCR4 have revealed that CXCL12-CXCR4 signaling is essential for the colonization of bone marrow by hematopoietic cells, including HSCs during ontogeny, maintenance of HSCs in the adult bone marrow, and development of B cells and plasmacytoid DCs (pDCs).[23-30] A recent study has shown that CXCL12 induces NK-cell migration and that administration of CXCR4 antagonist AMD3100 induced the reduction of NK cells in the bone marrow and their increase in spleen and peripheral blood, suggesting that CXCL12 regulates the retention of NK cells in the bone marrow[31]; however, the in vivo role of the CXCL12-CXCR4 signaling in NK-cell development remains unclear.

Submitted April 16, 2010; accepted October 3, 2010. Prepublished online as *Blood* First Edition paper, October 13, 2010; DOI 10.1182/blood-2010-04-277897.

The online version of this article contains a data supplement.

The publication costs of this article were defrayed in part by page charge payment. Therefore, and solely to indicate this fact, this article is hereby marked "advertisement" in accordance with 18 USC section 1734.

In this study, we have shown that CXCL12-CXCR4 chemokine signaling is dispensable for NK-cell development during ontogeny but plays a critical role in the generation of NK cells in adults.

Methods

Mice

CXCR4$^{null/null}$ mice,[25] CXCL12-GFP knock-in mice,[28] and CXCR4$^{flox(f)/null}$ mice[32] were maintained on a C57BL/6-Ly5.2$^+$/Ly5.1$^-$ background. CXCR4$^{wt/null}$ mice were intercrossed to generate CXCR4$^{-/-}$ embryo. Fetal thymuses were obtained from day 15.5 or 17.5 embryo, and the genotypes were determined by polymerase chain reaction (PCR) analysis. CXCR4$^{f/null}$ mice were crossed with MxCre transgenic mice to generate Cre-mediated CXCR4 conditionally deficient mice as described.[29] For removal of floxed CXCR4 allele, the MxCre/CXCR4$^{f/null}$ mice were injected subcutaneously with polyinosinic acid-polycytidylic acid (pIpC; 20 μg/g body weight; GE Healthcare) 8 times every other day from 3 days after birth, and were analyzed at 12 to 15 weeks after final pIpC treatment. All animal experimentation was conducted in accordance with the guidelines of the Institute for Frontier Medical Sciences, Kyoto University.

Antibodies

The following antibodies were used for flow cytometry: anti-CD3ε (145-2C11), anti-CD4 (RM4-5), anti-CD8a (53-6.7), anti-NK1.1 (PK136), anti-CD49b (DX5), anti-CD122 (TMβ1), anti-CD44 (IM7), anti-CD25 (7D4), anti-CD11b (M1/70), anti-CD27 (LG.3A10), anti-KLRG1 (2F1), anti-Ly49A (A1), anti-Ly49C/I (5E6), anti-Ly49D (4E5), anti-Ly49G2 (LGL-1), anti-CD94 (18d3), anti–IFN-γ (XMG1.2), anti–c-kit (2B8), anti–Sca-1 (D7), anti-Flt3 (A2F10), anti-CD45R (RA3–6B2), anti–Gr-1 (RB6–8C5), anti–TER-119 (TER-119), anti-CD19 (1D3), anti-Ly5.2 (104), anti-Ly5.1 (A20), CD31 (MEC13.3), CD11c (HL3), and major histocompatibility complex (MHC) class II (M5/114.15.2). All of these antibodies were directly conjugated to fluorescein isothiocyanate, phycoerythrin, phycoerythrin-Cy7, allophycocyanin, allophycocyanin-Cy7, Pacific blue, or biotin and were purchased from BD Biosciences or eBioscience. Biotinylated antibodies were detected with phycoerythrin-Cy7 (BD Biosciences) or Pacific blue (Invitrogen)–conjugated streptavidin.

Flow cytometric analysis and cell sorting

Single-cell suspensions were prepared from freshly isolated fetal thymus, adult bone marrow, spleen, lung, and peripheral blood. Cells were stained with monoclonal antibodies against cell surface markers and its secondary reagents. Dead cells were excluded by propidium iodide staining. All flow cytometric analysis and cell sorting were performed with FACSAria (BD Biosciences). For intracellular IFN-γ staining, single-cell suspensions from spleen were incubated at 1×10^6 cells/mL in 48-well plate in RPMI 1640 supplemented with 10% fetal calf serum (FCS; SAFC Biosciences), 50μM 2-mercaptoethanol, 50 μg/mL streptomycin, 75 μg/mL penicillin, 1 ng/mL IL-12 (PeproTech), 10 ng/mL IL-18 (MBL). After 2 hours of incubation, 10 μg/mL brefeldin A (Sigma-Aldrich) was added and incubated for an additional 4 hours. Fixation and permeabilization were performed with Cytofix/Cytoperm solution (BD Biosciences), followed by intracellular staining with allophycocyanin-conjugated anti–IFN-γ. Cell-cycle analysis was performed as described in our previous publication.[29] For the apoptosis assay, annexin V–FITC Apoptosis Detection Kit I (BD Biosciences) was used according to the manufacturer's instruction. For sorting the nonhematopoietic cell populations, cells in bone marrow fraction were obtained from femurs and tibiae by flushing and collagenase (Sigma-Aldrich) digestion.

Migration assay

Chemotactic migration assays with or without CXCL12 (200 μg/mL) were performed in 5-μm pore Transwell inset (Corning Life Sciences). Cells from bone marrow and spleen (5×10^5) were loaded on the upper well. After 90 minutes, the migrated cells from the lower well were harvested and analyzed by FACSAria.

Competitive repopulation assay

The competitive repopulation assay was performed as previously described.[29] Briefly, unfractionated 2×10^6 bone marrow cells from Ly5.2$^+$/Ly5.1$^-$ MxCre-CXCR4$^{f/wt}$ or MxCre-CXCR4$^{f/null}$ mice were mixed with 1×10^6 bone marrow cells from C57BL/6-Ly5.2$^-$/Ly5.1$^+$ mice as competitor cells and were transferred into lethally irradiated (9 Gy) C57BL/6-Ly5.2$^-$/Ly5.1$^+$ recipient mice. Mice were treated with pIpC at 12 weeks after transfer and were analyzed by flow cytometry at 15 weeks after final pIpC treatment.

Cytotoxicity assay

Lactate dehydrogenase (LDH) release assay was used to measure NK lytic activity against the NK-sensitive target YAC-1 cells in vitro. A total of 3×10^3 target cells were incubated with serially diluted effector cells in 0.1 mL of complete medium (RPMI 1640 supplemented with 2% FCS, 50μM 2-mercaptoethanol, 50 μg/mL streptomycin, 75 μg/mL penicillin) for 4 hours. Effector cells were bone marrow DX5$^+$ cells from 17-week-old mice that were enriched by positive selection with MACS DX5 microbeads (Miltenyi Biotec) or CD3$^-$NK1.1$^+$ cells that were sorted (> 99%) from bone marrow and spleen of 12-week-old mice by flow cytometry. LDH released on cell lysis was measured by Non-Radioactive Cytotoxicity Assay (CytoTox96; Promega) according to the manufacturer's instructions. The percentage of specific lysis was calculated as follows: 100 × (experimental − effector spontaneous − target spontaneous)/(target maximum − target spontaneous).

In vitro culture

Lin$^-$Sca-1$^+$c-kit$^+$Flt3$^+$ cells (LMPPs) (100 cells/well) and CD3$^-$NK1.1$^+$DX5$^-$ iNK cells (2000-3000 cells/well) sorted from bone marrow were cultured in 96-well U-bottomed plates in 0.1 mL of complete medium (RPMI 1640 with 10% FCS, 50μM 2-mercaptoethanol, 50 μg/mL streptomycin, 75 μg/mL penicillin, sodium pyruvate, and nonessential amino acids). For culture initiated with LMPPs, Flt3L, SCF (R&D Systems), IL-15 (PeproTech), and CXCL12 were used at 10 ng/mL, 20 ng/mL, and 1 μg/mL, respectively. The numbers of CD3$^-$NK1.1$^+$ NK cells were measured by flow cytometry on day 14 of culture. For culture initiated with iNKs, IL-15 and CXCL12 were used at 10 ng/mL and 1 μg/mL, respectively. The numbers of CD3$^-$NK1.1$^+$DX5$^+$ mNK cells were measured by flow cytometry on day 3 of culture.

Quantitative RT-PCR analysis

Total RNA was extracted from sorted cells with Isogen (Nippon Gene). After DNaseI (Invitrogen) treatment, reverse transcription was performed using SuperScript VILO cDNA Synthesis Kit (Invitrogen) according to the manufacturer's instructions. Quantitative PCR analysis was performed with a Step One Plus (Applied Biosystems) using Power SYBR Green PCR Master Mix (Applied Biosystems). Values for each gene were normalized to the relative quantity of glyceraldehyde-3-phosphate dehydrogenase (GAPDH) mRNA in each sample. The sequences of the primers used for the PCR reaction are as follows: GAPDH F, 5′-TCATGAGCCCTTCCACAATG-3′; GAPDH R, 5′-GGTGTGAACCACGAGAAATATGAC-3′; Perforin F, 5′-AAGGTAGCCAATTTTGCAGC-3′; Perforin R, 5′-GGTTTTTGTACCAGGCGAAA-3′; E4BP4 F, 5′-CGGAAGTTGCATCTCAGTCA-3′; E4BP4 R, 5′-GCAAAGCTCTCCAACTCCAC-3′; CXCR4 F, 5′-TAGGATCTTCCTGCCCACCAT-3; CXCR4 R, 5′-TGACCAGGATCACCAATCCA-3′; IL-15 F, 5′-ACATCCATCTCGTGCTACTTGT-3′; IL-15 R, 5′-GCTCGCATGCAGTCAGGAC-3′; IL-15Rα F, 5′-GCTTTCCTGGCCTGGTACATC-3′; and IL-15Rα R, 5′-CTGCTGGCCCTCACAGTCAT-3′.

Single-cell RT-PCR analysis

Single cells were sorted into reverse transcription buffer containing 1 U/μL RNase Inhibitor (Toyobo) and 0.4% Nonidet P-40 (Nacalai Tesque) using

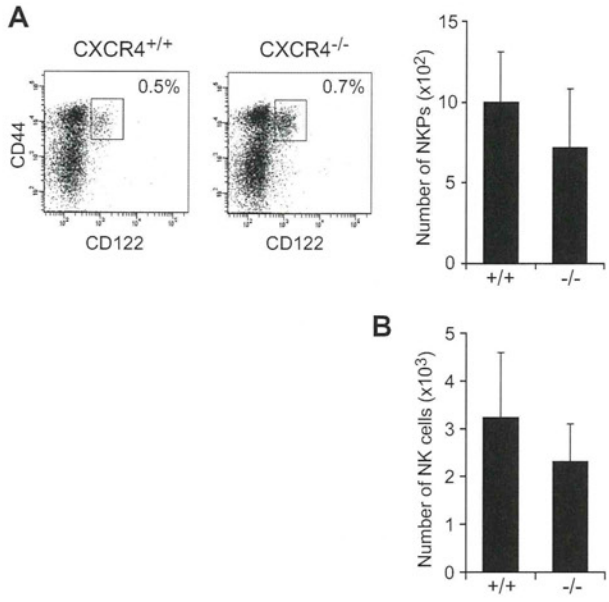

Figure 1. Normal cell numbers of NK cells in CXCR4-deficient fetal thymus. Flow cytometric analysis of NKPs and NK cells in CXCR4$^{null/null}$ fetal thymus. (A) Fluorescence staining profile of Lin$^-$ (TER119$^-$Mac-1$^-$Gr-1$^-$B220$^-$CD3$^-$CD4$^-$CD8$^-$) NK1.1$^-$CD25$^-$ cells (left) and the numbers of Lin$^-$NK1.1$^-$CD44$^+$CD25$^-$CD122$^+$ NKPs (right) in E15.5 fetal thymus. (B) The numbers of CD3$^-$NK1.1$^+$DX5$^+$ mNKs in E17.5 fetal thymus; n = 4.

flow cytometry. Cell lysates were reverse-transcribed using Moloney murine leukemia virus reverse transcriptase (Toyobo) and gene-specific reverse primers. PCR was subsequently performed by the addition of premixed hot-start PCR enzymes and buffers (AmpliTaq Gold, Applied Biosystems) containing the gene-specific forward and reverse primers designed to span introns to exclude genomic products. PCR was carried out in one round with 50 amplification cycles. A total of 100 cells per mouse were analyzed.

Immunohistochemical analysis

Immunostaining was performed as previously described.[29] In brief, 7-μm-thick 4% paraformaldehyde-fixed cryostat sections were first blocked with 5% FCS/phosphate-buffered saline and stained with goat anti–mouse NKp46 (R&D Systems), followed by secondary donkey anti–goat IgG-Cy3 (Jackson ImmunoResearch Laboratories). Sections were visualized with a LSM 510 META (Carl Zeiss) using a 40×/1.3 NA oil-immersion objective lens (Carl Zeiss). All acquired images were processed with the LSM Image Browser (Carl Zeiss).

Statistical analysis

Data were expressed as mean plus or minus SD. The statistical significances between groups were evaluated using the 2-tailed Student *t* test.

Results

CXCR4-CXCL12 signaling is required for NK-cell development in adults but not in embryos

To determine the in vivo role of CXCL12-CXCR4 signaling in NK-cell development, we first analyzed the numbers of NK-cell progenitors in CXCR4$^{null/null}$ embryos. A previous study showed that the numbers of p-T/NKs in the fetal liver were unaffected in CXCL12-deficient embryos.[27] Flow cytometric analysis of fetal thymocytes revealed no significant differences in the numbers of Lin$^-$NK1.1$^-$CD44$^+$CD25$^-$CD122$^+$ NKPs (Figure 1A) and CD3$^-$NK1.1$^+$DX5$^+$ mNKs (Figure 1B) between wild-type and CXCR4$^{null/null}$ embryos, suggesting that the CXCL12-CXCR4 signaling is dispensable for NK-cell development in embryos. Because conventional CXCR4$^{null/null}$ mice die in the embryonic stage, we next analyzed the bone marrow of MxCre/CXCR4$^{f/null}$ mice, in which Cre was expressed after the induction of type I IFN by the administration of pIpC to inactivate the CXCR4 gene in the adult animals.[29] In CXCR4 conditionally deficient mice, the numbers of CLPs in the bone marrow were severely reduced compared with control animals.[30] Flow cytometric analysis revealed that, although the numbers of T-cell precursors, including CD4$^-$CD8$^-$ (DN) and CD4$^+$CD8$^+$ (DP) cells in the thymus, were relatively unimpaired (supplemental Figure 1, available on the *Blood* Web site; see the Supplemental Materials link at the top of the online article), the numbers of NK-cell precursors, including Lin$^-$NK1.1$^-$DX5$^-$CD122$^+$ NKPs and CD3$^-$NK1.1$^+$DX5$^-$ iNKs, were reduced in the bone marrow of pIpC-treated MxCre/CXCR4$^{f/null}$ mice compared with pIpC-treated or untreated MxCre/CXCR4$^{f/wt}$ mice (Figure 2A; supplemental Figure 2). In addition, the frequencies and numbers of CD3$^-$NK1.1$^+$DX5$^+$ mNKs, including Mac-1$^-$ and Mac-1$^+$ subsets in the bone marrow (Figure 2A) and mNKs in the spleen, lung, and peripheral blood (Figure 2B; supplemental Figure 2; and data not shown), were more severely reduced in pIpC-treated MxCre/CXCR4$^{f/null}$ mice compared with control animals. Of note, the numbers of CD27$^+$Mac-1$^+$ (KLRG1$^-$) subset of mNKs, which are thought to display a greater effector function,[33] and KLRG1$^+$ end-stage mNKs[34] were severely reduced in bone marrow and spleen of pIpC-treated MxCre/CXCR4$^{f/null}$ mice (Figure 2C-D; and data not shown). In the mutants, expression of CXCR4 mRNA and migratory response to CXCL12 observed in NK cells from CXCR4 deleted mice was severely reduced as expected (supplemental Figure 3). Most Ly49 NK cell receptors exhibited normal expression levels, although inhibitory receptor Ly49G2 was abnormally expressed in CD3$^-$NK1.1$^+$ NK cells from the bone marrow of pIpC-treated MxCre/CXCR4$^{f/null}$ mice (Figure 2D). Perforin is a key effector molecule for NK cell–mediated cytolysis. Quantitative, real-time PCR with reverse transcription (RT) analysis revealed that the expression of Perforin was reduced in mNKs from the bone marrow and spleen of pIpC-treated MxCre/CXCR4$^{f/null}$ mice compared with pIpC-treated MxCre/CXCR4$^{f/wt}$ mice (Figure 2E).

The effect of CXCR4 depletion on the proliferation and survival of NK cells was examined using in vivo assays. We determined the proportion of NK cells from pIpC-treated MxCre/CXCR4$^{f/null}$ mice that incorporate bromodeoxyuridine (BrdU) over a 3-day period and used annexin V to stain these cells. The frequencies of iNK-incorporated BrdU over this period were decreased (Figure 2F), although there is no significant increase in annexin V–positive apoptotic NK cells in the absence of CXCR4 (supplemental Figure 4), suggesting that CXCL12 promotes proliferation of iNKs.

A recent study has shown that transcription factor E4BP4 is preferentially expressed in NK cells as well as NKT cells and is essential for NK-cell development, but not for NKT-cell development.[35] Quantitative RT-PCR analysis revealed that E4BP4 mRNA expression was reduced in mNKs from the bone marrow of pIpC-treated MxCre/CXCR4$^{f/null}$ mice compared with pIpC-treated MxCre/CXCR4$^{f/wt}$ mice (Figure 2G). This supports the idea that CXCR4 is essential for development of NK lineage and raises the possibility that CXCL12-CXCR4 signaling is involved in E4BP4 up-regulation in NK lineage cells.

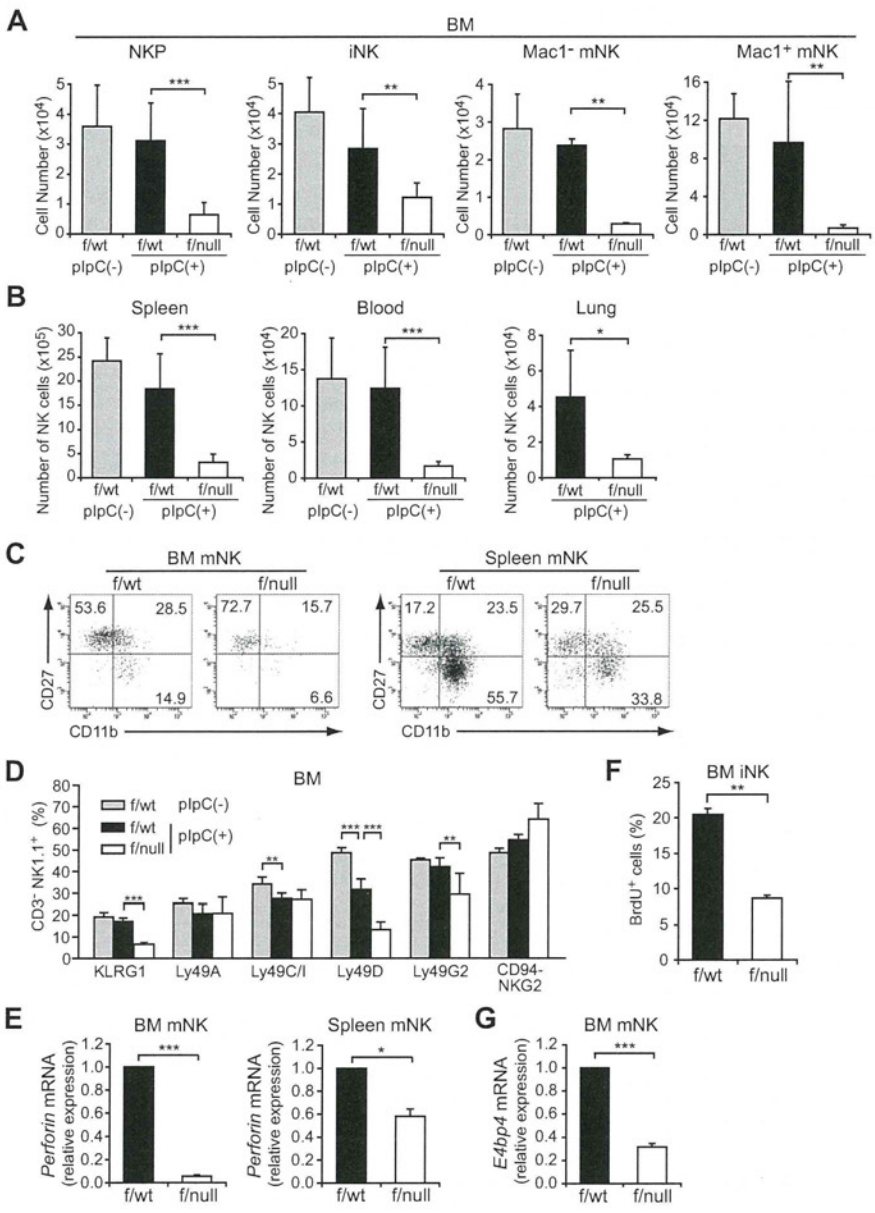

Figure 2. The severe developmental defect of NK cells in CXCR4 conditionally deficient mice. (A-D) Flow cytometric analysis of the numbers of Lin⁻ (TER119⁻Mac-1⁻Gr-1⁻ CD3⁻CD4⁻CD8⁻) NK1.1⁻DX5⁻CD122⁺ NKPs, CD3⁻NK1.1⁺DX5⁻ iNKs, and Mac-1⁻ and Mac-1⁺ subsets of CD3⁻NK1.1⁺DX5⁺ mNKs in the bone marrow (2 femurs and tibiae) (A), and CD3⁻NK1.1⁺DX5⁺ mNKs in spleen, lung, and peripheral blood (B) from untreated MxCre/CXCR4$^{f/wt}$, pIpC-treated MxCre/CXCR4$^{f/wt}$, or MxCre/CXCR4$^{f/null}$ mice; n = 4. (C) Immunofluorescent profiles of NK cells. Gated CD3⁻NK1.1⁺DX5⁺ are analyzed for the expression of Mac-1 and CD27. (D) Flow cytometric analysis of the frequencies of bone marrow CD3⁻NK1.1⁺ NK cells expressing KLRG1, Ly49A, C/I, D, G2, or CD94/NKG2; n = 4. (E,G) Quantitative RT-PCR analysis of mRNA expression of Perforin in CD3⁻NK1.1⁺DX5⁺ mNKs in the bone marrow and spleen (E) and E4BP4 in mNKs in the bone marrow (G) from pIpC-treated MxCre/CXCR4$^{f/wt}$ or MxCre/CXCR4$^{f/null}$ mice. Results are expressed as fold difference compared with the levels found in samples from MxCre/CXCR4$^{f/wt}$ mice (GAPDH normalization); n = 3. (F) BrdU was administered over a 3-day period. The frequencies of CD3⁻NK1.1⁺DX5⁻ iNKs incorporated BrdU over this period were analyzed by flow cytometry; n = 3. $^{*}P < .05$. $^{**}P < .01$. $^{***}P < .001$.

Next, to determine the numbers of functional NK cells, we assessed the capacity of freshly isolated NK cells to lyse YAC-1 targets in a LDH release assay and to produce IFN-γ in response to IL-12 and IL-18. In pIpC-treated MxCre/CXCR4$^{f/null}$ mice, NK cells from bone marrow showed reduced cytotoxicity against YAC-1 targets (Figure 3A), and NK cells from bone marrow and spleen contained decreased numbers of IFN-γ–producing cells (Figure 3B; and data not shown) compared with those from pIpC-treated MxCre/CXCR4$^{f/wt}$ mice. Considering the reduction in the number of CD3⁻NK1.1⁺ NK cells in CXCR4 conditionally deficient mice, these results indicate that the numbers of functional NK cells were severely reduced in the absence of CXCR4.

CXCR4 is required for NK-cell development in a cell-intrinsic manner

Our result that CXCR4 is essential for NK-cell development raised the question of whether the defect of NK-cell development in the absence of CXCR4 was attributed to an intrinsic NK lineage cell defect or to a microenvironmental defect. To address this issue, we injected 2×10^6 bone marrow cells from Ly5.2⁺/Ly5.1⁻ MxCre/CXCR4$^{f/wt}$ or MxCre/CXCR4$^{f/null}$ mice with or without 1×10^6 Ly5.2⁻/Ly5.1⁺ wild-type bone marrow hematopoietic cells into lethally irradiated wild-type Ly5.2⁻/Ly5.1⁺ mice. When chimeric mice exhibited long-term multilineage reconstitution by donor HSCs at 12 weeks after transfer, mice were treated with pIpC to induce excision of the floxed allele. At 15 weeks after final pIpC treatment, flow cytometric analysis revealed that the numbers of donor-derived NKPs, iNKs, and mNKs were severely reduced in the bone marrow from mutant chimeras with or without wild-type hematopoietic cells compared with control chimeras (Figure 4A; and data not shown). These results indicate that the defect of NK-cell development in the absence of CXCR4 is attributed to a cell-intrinsic CXCR4 deficiency. Consistent with this, CXCR4 mRNA is expressed in NKPs, iNKs, and mNKs from wild-type bone marrow (Figure 4B). Differences in the expression levels of CXCR4 mRNA between NKPs, iNKs, and mNKs are not statistically significant, although previous reports have shown a progressive reduction of cell surface expression level during maturation.[31,33] Cell surface expression

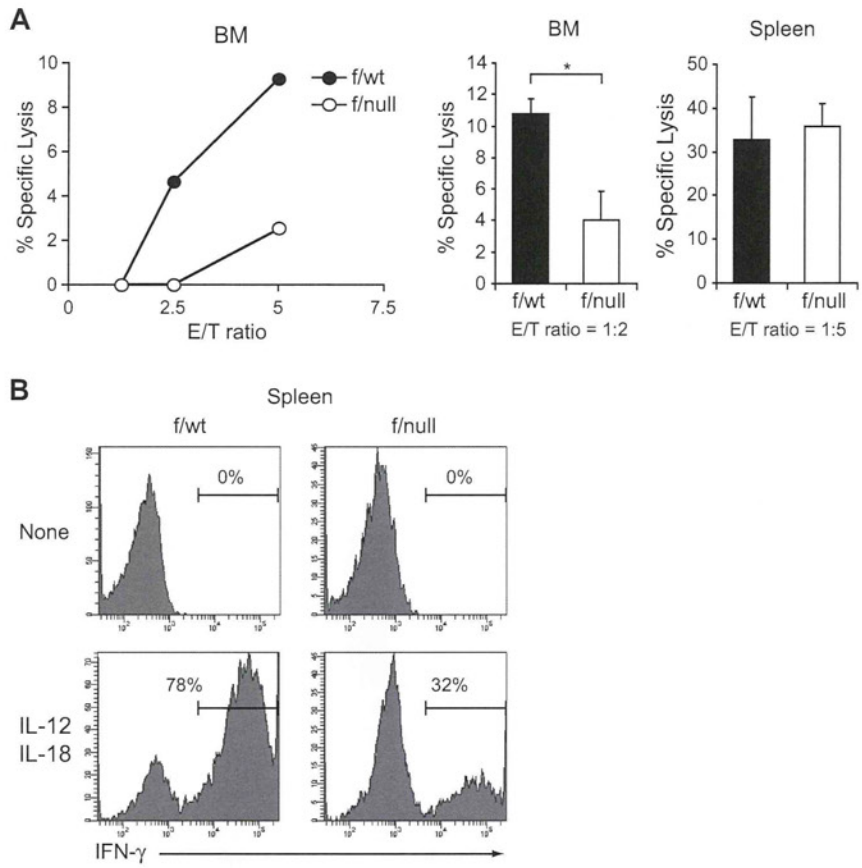

Figure 3. Decreased functional NK cells in CXCR4 conditionally deficient mice. (A) In vitro cytotoxicity of NK cells in the bone marrow (left and middle) or spleen (right) from pIpC-treated MxCre/CXCR4$^{f/wt}$ or MxCre/CXCR4$^{f/null}$ mice. LDH release assay was used to measure NK lytic activity against the NK cell-sensitive YAC-1 target cells. DX5$^+$ cells purified by magnetic-activated cell sorting (left) and sorted CD3$^-$NK1.1$^+$ NK cells (middle and right) were used as effector cells and were incubated with YAC-1 target cells at the indicated effector-to-target cell ratios (E/T) for 4 hours. Data are representative of 3 experiments; n = 3. *$P < .05$. (B) Flow cytometric analysis of in vitro IFN-γ production by NK cells in the spleen from pIpC-treated MxCre/CXCR4$^{f/wt}$ or MxCre/CXCR4$^{f/null}$ mice. Splenocytes were stimulated with IL-12 and IL-18 for 6 hours. IFN-γ production was measured in CD3$^-$NK1.1$^+$ NK cells by intracellular staining.

of CXCR4 in mNK cells might be down-regulated by ligand-induced receptor internalization.

In vitro effect of CXCL12 on generation of NK cells from LMPPs and iNKs

It has been reported previously that Lin$^-$ Sca-1$^+$c-kit$^+$ (LSK) Flt3^{hi} LMPPs are the first lymphoid-primed progenitors that give rise to NK cells in vitro and in vivo.[7] We examined the in vitro activities of CXCL12 in the generation of NK cells from LMPPs and the generation of mNKs from iNKs. LSK Flt3^{hi} and CD3$^-$NK1.1$^+$DX5$^-$ cells were sorted from the bone marrow of wild-type mice and cultured in medium containing Flt3L, SCF, and IL-15, which have been reported to be involved in NK-cell development in vivo,[12-16,22] in culture initiated with LMPPs or IL-15 in culture initiated with iNKs in the absence or presence of CXCL12. The numbers of NK cells were markedly increased with the addition of CXCL12 after 14-day culture initiated with LMPPs (Figure 5A). In addition, the numbers of CD3$^-$NK1.1$^+$DX5$^+$ mNKs were increased but to a lesser extent with the addition of CXCL12 after 3-day culture initiated with iNKs (Figure 5B). These results support the idea that CXCL12 is involved in the generation of NK cells from LMPPs and iNKs.

NK cells are associated with CAR cells in bone marrow

It has been shown previously that IL-15 is essential for the development and functional maturation of NK cells.[12] Thus, the result that CXCL12 is predominantly expressed in a small population of reticular cells, termed CXCL12-abundant reticular (CAR) cells in the bone marrow,[29,32] prompted us to examine the expression of IL-15 in CAR cells. It has been reported previously that IL-15 is expressed in bone marrow nonhematopoietic radiation-resistant cells, DCs, and activated monocytes.[36,37] Quantitative RT-PCR analysis of bone marrow from mice with the GFP reporter gene knocked into the CXCL12 locus (CXCL12-GFP knock-in mice)[28,29,32] revealed that the expression of IL-15 was considerably higher in CXCL12-GFP^{hi} CAR cells than in CXCL12-GFP$^-$ nonhematopoietic cells, CD11c^{high} MHC class II^{high} DCs, and Gr-1^{lo}Mac-1$^+$ myeloid lineage cells (Figure 6A). In addition, it has been reported previously that the expressions of IL-15 and IL-15Rα by the same cells support NK-cell maintenance.[38,39] Quantitative RT-PCR analysis of bone marrow from CXCL12-GFP knock-in mice revealed that IL-15Rα was expressed in CAR cells as well as CD11c^{high} MHC class II^{high} DCs, Gr-1^{lo}Mac-1$^+$ monocytes, and CD45$^-$CD31$^+$ endothelial cells (Figure 6B). Single-cell RT-PCR analysis revealed that all individual cells within the CAR cell population expressed IL-15 but only 26% of individual cells within the CAR cell population expressed IL-15Rα (Figure 6C). We next analyzed the association of NK cells with CAR cells in the bone marrow from pIpC-treated MxCre/CXCR4$^{f/null}$-CXCL12-GFP knock-in mice and control CXCR4$^{wt/wt}$-CXCL12-GFP knock-in mice. Immunohistochemical analysis with an antibody against NK-cell marker NKp46[40] revealed that most NK cells were in contact with the processes of CAR cells but at a distance from c-kit$^+$Sca-1$^+$ primitive hematopoietic cells or pDCs in pIpC-treated MxCre/CXCR4$^{f/null}$-CXCL12-GFP knock-in mice (data not shown) and control CXCR4$^{wt/wt}$-CXCL12-GFP knock-in mice (280 of 341; 82%) (Figure 6D). These results suggest that CAR cells, which produce both CXCL12 and IL-15, act as a microenvironmental niche for NK-cell development, but CXCL12-CXCR4 signaling is not essential for the association of NK cells with CAR cells in the bone marrow.

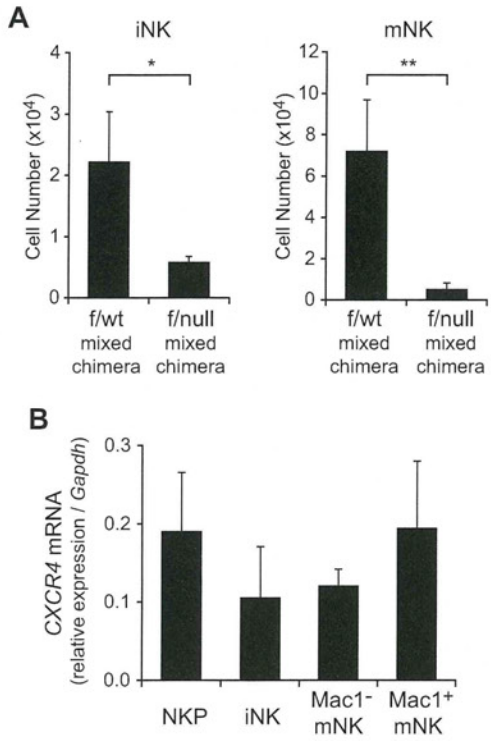

Figure 4. The developmental defect of NK cells in CXCR4 conditionally deficient mice is cell-intrinsic. Ly5.2$^+$/Ly5.1$^-$ bone marrow cells from MxCre/CXCR4$^{f/wt}$ or MxCre/CXCR4$^{f/null}$ mice were mixed with Ly5.2$^-$/Ly5.1$^+$ wild-type bone marrow cells and transplanted into lethally irradiated normal Ly5.2$^-$/Ly5.1$^+$ wild-type recipients. At 12 weeks after transplantation, mice were treated with pIpC. At 15 week after final pIpC treatment, recipient mice were analyzed by flow cytometry. (A) The numbers of donor-derived Ly5.2$^+$CD3$^-$NK1.1$^+$DX5$^-$ iNKs and Ly5.2$^+$CD3$^-$NK1.1$^+$DX5$^+$ mNKs; n = 4. *$P < .05$. **$P < .01$. (B) Quantitative RT-PCR analysis of mRNA expression of CXCR4 in NKPs, CD3$^-$NK1.1$^+$DX5$^-$ iNKs, and CD3$^-$NK1.1$^+$DX5$^+$ mNKs in the bone marrow from wild-type mice. Data are normalized to GAPDH levels; n = 3.

Discussion

This study has demonstrated that CXCL12-CXCR4 chemokine signaling is essential for the development of NK cells in adults. Both T cells and NK cells are thought to be generated from HSCs and CLPs, which require CXCR4; however, the numbers of T-cell precursors were relatively unimpaired, but the numbers of NKPs and iNKs were reduced and the numbers of mNKs were more severely reduced in the bone marrow of CXCR4 conditionally deficient mice compared with control mice. Together with the findings that the numbers of mNKs were also reduced in the spleen and peripheral blood of CXCR4 conditionally deficient mice and that CXCL12 enhanced the generation of mNKs from iNKs in culture, our results suggest that CXCL12-CXCR4 signaling plays a critical role in the generation of NK lineage cells within the bone marrow. In addition, the results that the frequencies of iNKs incorporated BrdU over a 3-day period were decreased in the absence of CXCR4 suggest that CXCL12 promotes proliferation of iNKs in the marrow.

Furthermore, the possibility that the reduction in NK cells that is observed after CXCR4 deletion may be the result of a reduction in DC subsets that provide transpresented IL-15 for NK-cell development and homeostasis[36-39] appears unlikely because the numbers of CXCR4-deficient NK cells were severely reduced in the bone marrow of chimeric mice reconstituted with both CXCR4-deficient and wild-type hematopoietic cells.

In contrast to the bone marrow, NK cells do not require CXCL12 in fetal ontogeny. This supports the idea that HSCs present in fetal life give rise to different sets of lymphohematopoietic progenitors that require different cytokines than HSCs present in adult bone marrow.

Although essential signals downstream of CXCR4 in hematopoiesis remain unclear, recent studies have suggested that phosphoinositide 3-kinases (PI3Ks), PI3Kδ and PI3Kγ, which catalyze the phosphorylation of the 3′ hydroxyl group of phosphoinositides, generating PI(3,4,5)P3 are activated by G protein βγ subunits and downstream effectors of CXCR4 in β-selection during T-cell development.[41] Of note, mice lacking PI3K catalytic subunits, p110γ and p110δ, had normal numbers of B cells but severely reduced numbers of mNK in the bone marrow and spleen,[42] suggesting that in NK-cell development, but not in B-cell development, PI3Kδ and PI3Kγ serve as critical downstream regulators of CXCR4 signaling in the bone marrow.

Although IL-15 is known to be essential for development and functional maturation of NK cells, cellular sources of IL-15 in the bone marrow during homeostasis remain unclear. On the other hand, it has been reported previously that IL-15 and its receptor IL-15Rα are coexpressed by the same cells, which transpresent IL-15 to NK cells during development,[38,39] and that lethally irradiated IL-15Rα–deficient mice reconstituted with wild-type bone marrow cells had decreased numbers of NK cells, indicating that IL-15Rα in nonhematopoietic cells is essential for NK-cell development.[43] In addition, although IL-15 is expressed in DCs and monocytes,[36,37] the expression of IL-15Rα by DCs and monocytes was dispensable for NK-cell development in the bone marrow.[44] Thus, the results that mRNA expression of IL-15 and CXCL12 was considerably higher in CAR cells than in other nonhematopoietic cells, that CAR cells express IL-15Rα and that most NK cells were in contact with the processes of CAR cells suggest that CAR cells provide IL-15 and CXCL12 and function as a niche for NK-cell development in the bone marrow. In contrast to IL-15 and CXCL12, IL-15Rα was expressed in only 26% of individual CAR cells, raising the possibility that CAR cells expressing IL-15Rα create a specific niche for NK cells. Together with previous studies, our findings

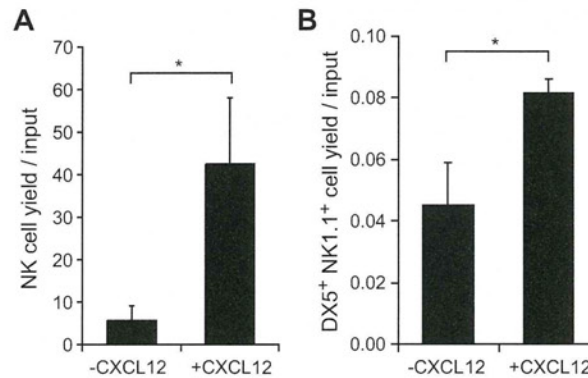

Figure 5. In vitro effects of CXCL12 on generation of NK cells from LMPPs or iNKs. (A) Sorted Lin$^-$Sca-1$^+$c-kit$^+$ (LSK) Flt3^{hi} LMPPs were cultured in medium containing Flt3L, SCF, and IL-15 in the absence or presence of CXCL12. After 14-day culture, CD3$^-$NK1.1$^+$ NK cells were counted by flow cytometry; n = 4. *$P < .05$. (B) Sorted CD3$^-$NK1.1$^+$DX5$^-$ iNKs were cultured in medium containing IL-15 in the absence or presence of CXCL12. After 3-day culture, the number of CD3$^-$NK1.1$^+$DX5$^+$ mNKs were measured by flow cytometry; n = 4. *$P < .05$.

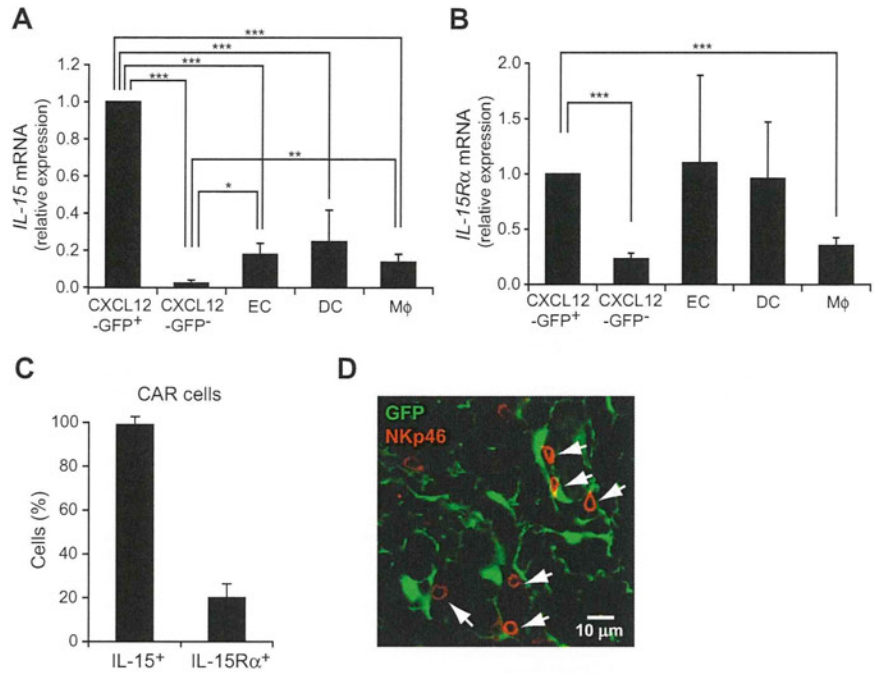

Figure 6. The expression of IL-15 in CAR cells and their association with NK cells in bone marrow. (A-B) Quantitative RT-PCR analysis of mRNA expression of IL-15 (A) and IL-15Rα (B) in CXCL12-GFP^{hi} (CAR) cells, CD45$^-$CXCL12-GFP$^-$ nonhematopoietic cells, CD45$^-$CD31$^+$ endothelial cells (EC), CD11c^{high} MHC class II^{high} DCs, and Gr-1^{lo}Mac-1$^+$ myeloid lineage cells (Mϕ) in the bone marrow from wild-type mice or CXCL12-GFP knock-in mice. (C) Single-cell RT-PCR analysis of the frequencies of cells expressing IL-15 or IL-15Rα in sorted CAR cells; n = 3. (D) The bone marrow sections from CXCL12-GFP knock-in mice were stained with antibodies against NKp46 (red). Most NKp46$^+$ NK cells are in contact with CAR cells (green). *$P < .05$. **$P < .01$. ***$P < .001$.

suggest that CAR cells function as niches for various types of hematopoietic cells, including HSCs, B cells, pDCs, and NK cells in the bone marrow. However, histologic analysis revealed that NK cells were not located close to c-kit$^+$Sca-1$^+$ primitive hematopoietic cells or pDCs, raising the possibility that CAR cells are a common cellular component of distinct specific niches for HSCs, B cells, pDCs and NK cells.

This study demonstrates the novel role of CXCL12-CXCR4 chemokine signaling in immune cell development. Further studies will be needed to determine how the generation of NK cells, B cells, and pDCs is regulated in the presence of CXCL12 in niches in which CAR cells are implicated as a key component.

Acknowledgments

The authors thank H. Kohara (Institute for Frontier Medical Sciences, Kyoto University) for technical assistance.

This work was supported by the Ministry of Education, Science, Sports and Culture of Japan and the Uehara Memorial Foundation.

Authorship

Contribution: M.N. and T.N. designed and performed the experiments, analyzed the data, and prepared the paper; Y.O. and T.S. performed the experiments and analyzed the data; S.O. and N.F. contributed materials and tools; and T.N. supervised the study.

Conflict-of-interest disclosure: The authors declare no competing financial interests.

Correspondence: Takashi Nagasawa, Department of Immunobiology and Hematology, Institute for Frontier Medical Sciences, Kyoto University, 53 Kawahara-cho, Shogoin, Sakyo-ku, Kyoto 606-8507, Japan; e-mail: tnagasa@frontier.kyoto-u.ac.jp.

References

1. Yokoyama WM, Kim S, French AR. The dynamic life of natural killer cells. *Annu Rev Immunol.* 2004;22:405-429.
2. Di Santo JP. Natural killer cell developmental pathways: a question of balance. *Annu Rev Immunol.* 2006;24:257-286.
3. Kawamoto H, Ikawa T, Ohmura K, Fujimoto S, Katsura Y. T cell progenitors emerge earlier than B cell progenitors in the murine fetal liver. *Immunity.* 2000;12(4):441-450.
4. Rodewald HR, Moingeon P, Lucich JL, Dosiou C, Lopez P, Reinherz EL. A population of early fetal thymocytes expressing Fc gamma RII/III contains precursors of T lymphocytes and natural killer cells. *Cell.* 1992;69(1):139-150.
5. Ikawa T, Kawamoto H, Fujimoto S, Katsura Y. Commitment of common T/natural killer (NK) progenitors to unipotent T and NK progenitors in the murine fetal thymus revealed by a single progenitor assay. *J Exp Med.* 1999;190(11):1617-1626.
6. Carlyle JR, Michie AM, Cho SK, Zuniga-Pflucker JC. Natural killer cell development and function precede alpha beta T cell differentiation in mouse fetal thymic ontogeny. *J Immunol.* 1998;160(2):744-753.
7. Adolfsson J, Mansson R, Buza-Vidas N, et al. Identification of Flt3+ lympho-myeloid stem cells lacking erythro-megakaryocytic potential: a revised road map for adult blood lineage commitment. *Cell.* 2005;121(2):295-306.
8. Kondo M, Weissman IL, Akashi K. Identification of clonogenic common lymphoid progenitors in mouse bone marrow. *Cell.* 1997;91(5):661-672.
9. Karsunky H, Inlay MA, Serwold T, Bhattacharya D, Weissman IL. Flk2+ common lymphoid progenitors possess equivalent differentiation potential for the B and T lineages. *Blood.* 2008;111(12):5562-5570.
10. Rosmaraki EE, Douagi I, Roth C, Colucci F, Cumano A, Di Santo JP. Identification of committed NK-cell progenitors in adult murine bone marrow. *Eur J Immunol.* 2001;31(6):1900-1909.
11. Kim S, Iizuka K, Kang HS, et al. In vivo developmental stages in murine natural killer cell maturation. *Nat Immunol.* 2002;3(6):523-528.
12. Kennedy MK, Glaccum M, Brown SN, et al. Reversible defects in natural killer and memory CD8 T cell lineages in interleukin 15-deficient mice. *J Exp Med.* 2000;191(5):771-780.
13. Lodolce JP, Boone DL, Chai S, et al. IL-15 receptor maintains lymphoid homeostasis by supporting lymphocyte homing and proliferation. *Immunity.* 1998;9(5):669-676.
14. Suzuki H, Duncan GS, Takimoto H, Mak TW. Abnormal development of intestinal intraepithelial lymphocytes and peripheral natural killer cells in mice lacking the IL-2 receptor beta chain. *J Exp Med.* 1997;185(3):499-505.
15. DiSanto JP, Muller W, Guy-Grand D, Fischer A, Rajewsky K. Lymphoid development in mice with a targeted deletion of the interleukin 2 receptor gamma chain. *Proc Natl Acad Sci U S A.* 1995;92(2):377-381.
16. McKenna HJ, Stocking KL, Miller RE, et al. Mice lacking flt3 ligand have deficient hematopoiesis affecting hematopoietic progenitor cells, dendritic cells, and natural killer cells. *Blood.* 2000;95(11):3489-3497.
17. Kundig TM, Schorle H, Bachmann MF, Hengartner H,

Zinkernagel RM, Horak I. Immune responses in interleukin-2-deficient mice. *Science.* 1993;262(5136):1059-1061.

18. Vosshenrich CA, Ranson T, Samson SI, et al. Roles for common cytokine receptor gamma-chain-dependent cytokines in the generation, differentiation, and maturation of NK-cell precursors and peripheral NK cells in vivo. *J Immunol.* 2005;174(3):1213-1221.
19. Moore TA, von Freeden-Jeffry U, Murray R, Zlotnik A. Inhibition of gamma delta T cell development and early thymocyte maturation in IL-7 −/− mice. *J Immunol.* 1996;157(6):2366-2373.
20. He YW, Malek TR. Interleukin-7 receptor alpha is essential for the development of gamma delta + T cells, but not natural killer cells. *J Exp Med.* 1996;184(1):289-293.
21. Waskow C, Rodewald HR. Lymphocyte development in neonatal and adult c-Kit-deficient (c-KitW/W) mice. *Adv Exp Med Biol.* 2002;512:1-10.
22. Colucci F, Di Santo JP. The receptor tyrosine kinase c-kit provides a critical signal for survival, expansion, and maturation of mouse natural killer cells. *Blood.* 2000;95(3):984-991.
23. Nagasawa T. Microenvironmental niches in the bone marrow required for B-cell development. *Nat Rev Immunol.* 2006;6(2):107-116.
24. Nagasawa T, Hirota S, Tachibana K, et al. Defects of B-cell lymphopoiesis and bone-marrow myelopoiesis in mice lacking the CXC chemokine PBSF/SDF-1. *Nature.* 1996;382(6592):635-638.
25. Tachibana K, Hirota S, Iizasa H, et al. The chemokine receptor CXCR4 is essential for vascularization of the gastrointestinal tract. *Nature.* 1998;393(6685):591-594.
26. Zou YR, Kottmann AH, Kuroda M, Taniuchi I, Littman DR. Function of the chemokine receptor CXCR4 in haematopoiesis and in cerebellar development. *Nature.* 1998;393(6685):595-599.
27. Egawa T, Kawabata K, Kawamoto H, et al. The earliest stages of B cell development require a chemokine stromal cell-derived factor/pre-B cell growth-stimulating factor. *Immunity.* 2001;15(2):323-334.
28. Ara T, Tokoyoda K, Sugiyama T, Egawa T, Kawabata K, Nagasawa T. Long-term hematopoietic stem cells require stromal cell-derived factor-1 for colonizing bone marrow during ontogeny. *Immunity.* 2003;19(2):257-267.
29. Sugiyama T, Kohara H, Noda M, Nagasawa T. Maintenance of the hematopoietic stem cell pool by CXCL12-CXCR4 chemokine signaling in bone marrow stromal cell niches. *Immunity.* 2006;25(6):977-988.
30. Kohara H, Omatsu Y, Sugiyama T, Noda M, Fujii N, Nagasawa T. Development of plasmacytoid dendritic cells in bone marrow stromal cell niches requires CXCL12-CXCR4 chemokine signaling. *Blood.* 2007;110(13):4153-4160.
31. Bernardini G, Sciume G, Bosisio D, Morrone S, Sozzani S, Santoni A. CCL3 and CXCL12 regulate trafficking of mouse bone marrow NK cell subsets. *Blood.* 2008;111(7):3626-3634.
32. Tokoyoda K, Egawa T, Sugiyama T, Choi BI, Nagasawa T. Cellular niches controlling B lymphocyte behavior within bone marrow during development. *Immunity.* 2004;20(6):707-718.
33. Hayakawa Y, Smyth MJ. CD27 dissects mature NK cells into two subsets with distinct responsiveness and migratory capacity. *J Immunol.* 2006;176(3):1517-1524.
34. Huntington ND, Tabarias H, Fairfax K, et al. NK cell maturation and peripheral homeostasis is associated with KLRG1 up-regulation. *J Immunol.* 2007;178(8):4764-4770.
35. Gascoyne DM, Long E, Veiga-Fernandes H, et al. The basic leucine zipper transcription factor E4BP4 is essential for natural killer cell development. *Nat Immunol.* 2009;10(10):1118-1124.
36. Bamford RN, Battiata AP, Burton JD, Sharma H, Waldmann TA. Interleukin (IL) 15/IL-T production by the adult T-cell leukemia cell line HuT-102 is associated with a human T-cell lymphotrophic virus type I region /IL-15 fusion message that lacks many upstream AUGs that normally attenuates IL-15 mRNA translation. *Proc Natl Acad Sci U S A.* 1996;93(7):2897-2902.
37. Ruckert R, Brandt K, Bulanova E, Mirghomizadeh F, Paus R, Bulfone-Paus S. Dendritic cell-derived IL-15 controls the induction of CD8 T cell immune responses. *Eur J Immunol.* 2003;33(12):3493-3503.
38. Sandau MM, Schluns KS, Lefrancois L, Jameson SC. Cutting edge: transpresentation of IL-15 by bone marrow-derived cells necessitates expression of IL-15 and IL-15R alpha by the same cells. *J Immunol.* 2004;173(11):6537-6541.
39. Burkett PR, Koka R, Chien M, Chai S, Boone DL, Ma A. Coordinate expression and trans presentation of interleukin (IL)-15Ralpha and IL-15 supports natural killer cell and memory CD8+ T cell homeostasis. *J Exp Med.* 2004;200(7):825-834.
40. Walzer T, Blery M, Chaix J, et al. Identification, activation, and selective in vivo ablation of mouse NK cells via NKp46. *Proc Natl Acad Sci U S A.* 2007;104(9):3384-3389.
41. Janas ML, Varano G, Gudmundsson K, Noda M, Nagasawa T, Turner M. Thymic development beyond beta-selection requires phosphatidylinositol 3-kinase activation by CXCR4. *J Exp Med.* 2010;207(1):247-261.
42. Tassi I, Cella M, Gilfillan S, et al. p110gamma and p110delta phosphoinositide 3-kinase signaling pathways synergize to control development and functions of murine NK cells. *Immunity.* 2007;27(2):214-227.
43. Kawamura T, Koka R, Ma A, Kumar V. Differential roles for IL-15R alpha-chain in NK-cell development and Ly-49 induction. *J Immunol.* 2003;171(10):5085-5090.
44. Mortier E, Advincula R, Kim L, et al. Macrophage- and dendritic-cell-derived interleukin-15 receptor alpha supports homeostasis of distinct CD8+ T cell subsets. *Immunity.* 2009;31(5):811-822.

Organic & Biomolecular Chemistry

Dynamic Article Links

Cite this: *Org. Biomol. Chem.*, 2011, **9**, 3421

www.rsc.org/obc

PAPER

Design and synthesis of amidine-type peptide bond isosteres: application of nitrile oxide derivatives as active ester equivalents in peptide and peptidomimetics synthesis†

Eriko Inokuchi,[a] Ai Yamada,[a] Kentaro Hozumi,[b] Kenji Tomita,[a] Shinya Oishi,[a] Hiroaki Ohno,[a] Motoyoshi Nomizu[b] and Nobutaka Fujii*[a]

Received 17th December 2010, Accepted 16th February 2011
DOI: 10.1039/c0ob01193b

Amidine-type peptide bond isosteres were designed based on the substitution of the peptide bond carbonyl (C=O) group with an imino (C=NH) group. The positively-charged property of the isosteric part resembles a reduced amide-type peptidomimetic. The peptidyl amidine units were synthesized by the reduction of a key amidoxime (*N*-hydroxyamidine) precursor, which was prepared from nitrile oxide components as an aminoacyl or peptidyl equivalent. This nitrile oxide-mediated C–N bond formation was also used for peptide macrocyclization, in which the amidoxime group was converted to peptide bonds under mild acidic conditions. Syntheses of the cyclic RGD peptide and a peptidomimetic using both approaches, and their inhibitory activity against integrin-mediated cell attachment, are presented.

Introduction

The backbone modification of amide bonds **1** in bioactive peptides is one of the most promising approaches for improving their resistance towards degradation by peptidases.[1] A number of peptide bond isosteres that reproduce their electrostatic properties and secondary structure conformations have been reported.[2] Reduced amide bonds (–CH_2–NH–) **2** with a positively-charged secondary amine provide a flexible and hydrogen bond-donating substructure (Fig. 1). The success of this substructure is exemplified by several enzyme inhibitors of HIV-1 protease[3] and neuronal nitric oxide synthase.[4] Alkene dipeptide isosteres (–CR=CH–, R = H, F or Me) **3**[2,5] also represent steady-state peptide bond mimetics. This motif has been employed for the preparation of functional probes to identify indispensable peptide bonds. During the course of our medicinal chemistry studies using these isosteres, it has been demonstrated that a heavy atom corresponding to the carbonyl oxygen in peptide bonds favorably modulates local and global peptide conformations.[6]

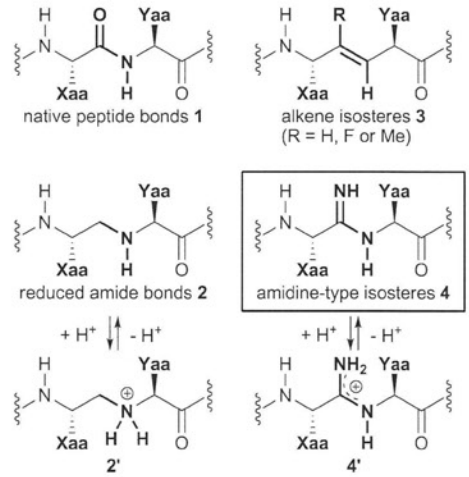

Fig. 1 Structures of the peptide bond and mimetics.

The uncharged form of amidines **4** resemble the peptide bond structure **1**, in which both imino and amino functional groups share an sp^2 carbon. Under physiological conditions, amidines are protonated and the positive charge of the conjugated acid is delocalized over two nitrogens. Characteristic substructure **4′** can be viewed as a modified motif of the peptide bond and/or reduced amide structure. However, there are few reports on amidine-type peptide bond isosteres **4**,[7,8] while acyclic amidines[9] and cyclic amidines[10] have been utilized as equivalents of the basic guanidino group for several bioactive molecules.

Whereas amidines have been synthesized directly by the Pinner reaction[7,8b] or by the coupling of imidyl chlorides with amines, these reactions are not applicable to peptidyl amidine synthesis because of the harsh reaction conditions or the arduous substrate preparation. We have postulated that amidoximes (*N*-hydroxyamidines) **8** represent an appropriate key precursor for peptidyl amidine synthesis, which are obtained by the coupling of nitrile oxides **6** with nucleophilic amines **7** (Scheme 1).[11] Reduction[10] or hydrolysis under mild acidic conditions[12] of the key

[a]*Graduate School of Pharmaceutical Sciences, Kyoto University, Sakyo-ku, Kyoto, 606-8501, Japan. E-mail: nfujii@pharm.kyoto-u.ac.jp; Fax: +81 75-753-4570; Tel: +81 75-753-4551*

[b]*School of Pharmacy, Tokyo University of Pharmacy and Life Sciences, 1432-1 Horinouchi, Hachioji, Tokyo, 192-0392, Japan*

† Electronic supplementary information (ESI) available. See DOI: 10.1039/c0ob01193b

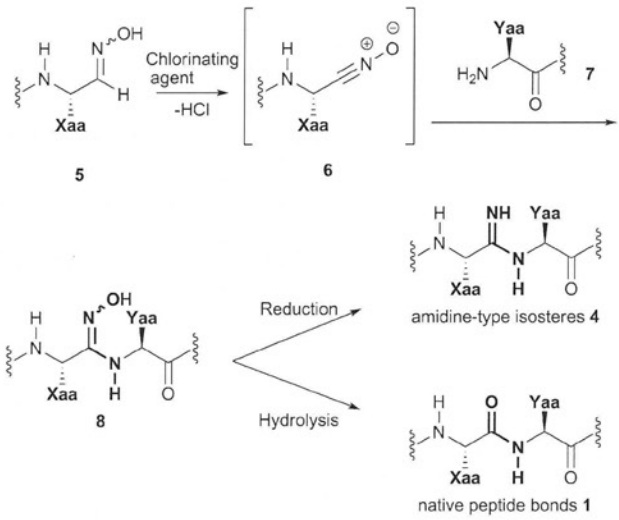

Scheme 1 Synthetic scheme for amidine-type peptide bond isosteres **4** and native peptide bonds **1** using nitrile oxides **6** as reactive acyl equivalents.

amidoximes **8** would provide the target peptidyl amidine **4** or the parent peptide bond **1**, respectively. It was also expected that highly reactive nitrile oxides **6** derived from peptide aldoximes **5** could be exploited as active ester equivalents for fragment condensation to prepare various protected peptides and peptidomimetics. Herein, we describe a novel approach for the synthesis of peptides and amidine-type peptidomimetics *via* peptide amidoximes.

Results and discussion

Preparation of amino acid-derived nitrile oxides and their application to the synthesis of peptide bond and amidine-type peptidomimetics

Nitrile oxides are useful reactive species that can be formed from aldoximes by treatment with a chlorinating agent and a weak base.[11] There have been a number of reports of 1,3-dipolar cycloadditions of nitrile oxides with olefins to produce isoxazoline derivatives,[13] whereas examples utilizing nitrile oxides as active ester equivalents are limited. We expected that α-aminoaldoximes and peptide aldoximes would serve as useful precursors of reactive nitrile oxide components for peptide and peptidomimetic synthesis.

Initially, we optimized the coupling conditions of α-aminoaldoxime **9**[14] and α-amino ester **12**. This consisted of a two-step process including chlorination of aldoxime **9** and the subsequent nucleophilic attack of amino ester **12** onto nitrile oxide **11**, derived from **10**, under basic conditions (Table 1). The major isomer of *N*-Boc-valine aldoxime, **9a**, reacted with an NaOCl solution[11] followed by work-up and treatment with amino ester **12** to give the desired amidoxime (*N*-hydroxyamidine) product, **13**, in 77% yield (Table 1, entry 1), while minor isomer **9b** produced a complex mixture of unidentified products with the same reagent (Table 1, entry 2). This was presumably due to the concomitant formation of unstable nitrile oxide **11** under the basic conditions of the first chlorination step. Treatment of both aldoxime isomers **9a** and **9b** with *N*-chlorosuccinimide (NCS) in DMF without base provided the same product, **13**, in satisfactory yields (Table 1, entries 3 and 4). Of note, the chlorination of **9a** with NCS in $CHCl_3$ did not work, resulting in the recovery of the starting material. As such, a facile protocol to prepare amidoximes from the both isomers of amino acid-derived aldoximes was established.

Conversion processes from amidoxime **13** were next investigated. The hydrogenation of **13** with RANEY® Ni[10] cleaved the N–O bond to afford the expected amidine-type isosteric unit, **14**, in 67% yield (Scheme 2). Alternatively, the hydrolysis of **13** under mild acidic conditions containing $NaNO_2$ gave the parent dipeptide unit, **15**, in 62% yield.[12] No epimerization of the amidoximes occurred during the coupling process, which was verified by comparing **15** with two authentic diastereomers prepared by the standard protocol for peptide synthesis.

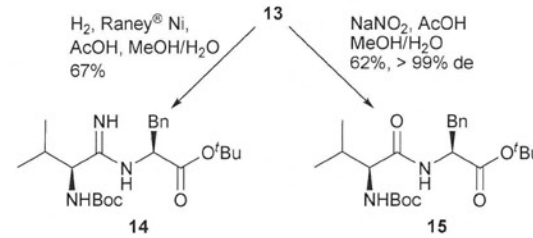

Scheme 2 Conversion of *N*-hydroxyamidine **13** to amidine **14** and peptide bond **15**.

Table 1 Optimization of the aldoxime–amino acid coupling conditions

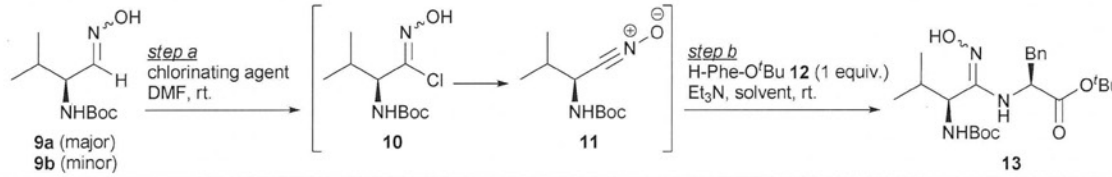

Entry	Substrate[a]	Step a	Step b	Yield (%)
1	**9a**	NaOCl[b] (3.0 equiv.), Et_3N (3.0 equiv.)	Et_3N (6.0 equiv.)/CH_2Cl_2	77
2	**9b**	NaOCl[b] (3.0 equiv.), Et_3N (3.0 equiv.)	Et_3N (6.0 equiv.)/CH_2Cl_2	Decomp.
3	**9a**	NCS (1.4 equiv.)	Et_3N (4.0 equiv.)/Et_2O	71[c]
4	**9b**	NCS (1.4 equiv.)	Et_3N (4.0 equiv.)/Et_2O	81

[a] Substrates **9** were prepared from Boc-valinal according to literature procedures.[14] [b] 30% aqueous solution. [c] When $CHCl_3$ was used as the reaction solvent in step a, starting material **9a** was recovered.

Table 2 Preparation of aldoxime resin **19**

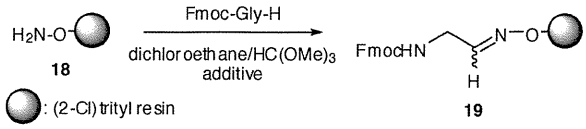

Entry	Additive (1.2 equiv.)	Conditions[a]	Loading (%)
1	—	rt, o/n	83
2	Et_3N	rt, o/n	56
3	AcOH	rt, o/n	90
4	AcOH	60 °C, o/n	99
5	AcOH	60 °C, 2 h	99

[a] Dichloroethane (0.15 M), $HC(OMe)_3$ (0.2 M).

Solid-phase synthesis of peptide aldoximes and the application of nitrile oxide-mediated coupling to cyclic peptide synthesis

The nitrile oxide-mediated synthesis of peptides and peptidomimetics was applied by a solid-phase approach. We chose cyclic RGD peptide **16**, *cyclo*(–Arg–Gly–Asp–D-Phe–Val–),[15] which is a highly potent integrin $\alpha_v\beta_3$ antagonist that includes two reactive side-chains (Arg and Asp), and mimetic **17** *cyclo*(–Arg–Gly–ψ[C(=NH)–NH]–Asp–D-Phe–Val–) as target peptides. We planned to synthesize RGD peptide **16** and peptidomimetic **17** by a nitrile oxide-mediated cyclization, followed by hydrolysis and hydrogenolysis, respectively. For application to solid-phase synthesis, the preparation of aldoxime resin **19** was investigated. The direct attachment of Fmoc-protected aminoaldoximes such as Fmoc–NH–CH_2–CH=NH–OH onto the (2-Cl)trityl chloride resin failed to afford the expected resin under any conditions. In contrast, resin **18** was prepared from the (2-Cl)trityl chloride resin and Fmoc-protected hydroxyamine (89% loading), followed by piperidine treatment. The reaction of an Fmoc-protected α-aminoaldehyde with aminooxy (2-Cl)trityl resin **18** gave the desired aldoxime resin, **19** (83% loading; Table 2, entry 1). An acidic additive improved the reactivity, and the reaction proceeded smoothly at 60 °C within 2 h to give aldoxime resin **19** in 99% yield (Table 2, entry 5).[16]

Peptide elongation was performed by the standard Fmoc-based solid-phase synthesis approach using *N*,*N*′-diisopropylcarbodiimide (DIC)/HOBt in DMF to give peptide aldoxime resin **20** (Scheme 3). During the solid-phase process, the oxime–ether linker was inert, even when treated with 20% piperidine in DMF for Fmoc removal. For peptide cleavage from the solid support, the standard conditions [30% 1,1,1,3,3,3-hexafluoropropan-2-ol (HFIP) in CH_2Cl_2, rt, 2 h[17]] were ineffective for aldoxime resin **20**, indicating that the oxime–ether linkage is less acid-labile compared with peptide acids and peptide alcohols. The treatment of resin **20** in TFA/triisopropylsilane (TIS)/CH_2Cl_2 (0.5/0.1/99.4) provided linear peptide aldoxime **21** in a quantitative yield.

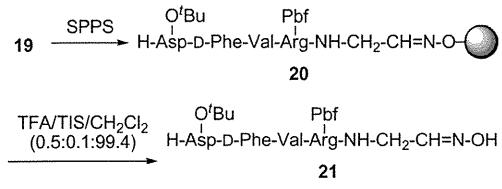

Scheme 3 Preparation of peptide aldoxime **21**.

Cyclization of acyclic peptide aldoxime **21** by treatment with NCS, followed by Et_3N, gave amidoxime-containing peptide **22** in a moderate yield (36%, Scheme 4). The yield of the aldoxime-mediated cyclization was comparable with approaches using the azide method or DPPA-mediated cyclizations (11–52% cyclization yields for the RGD peptide **16** and the derivatives).[15a] Subsequently, amidoxime **22** was converted smoothly to amide **23a** and amidine **23b** in 46 and 95% yields, respectively, by $NaNO_2$-mediated acidic hydrolysis and RANEY® Ni-mediated hydrogenation. The protecting groups for Arg and Asp were cleaved off using a cocktail of 1 M TMSBr–thioanisole/TFA in the presence of *m*-cresol and 1,2-ethanedithiol (EDT) in a short time, providing the desired parent RGD peptide **16** and peptidomimetic **17** in 87 and 73% yields, respectively. It is of note that no hydrolyzed product **16** was observed during the deprotection treatment of **23b** and subsequent HPLC purification process.

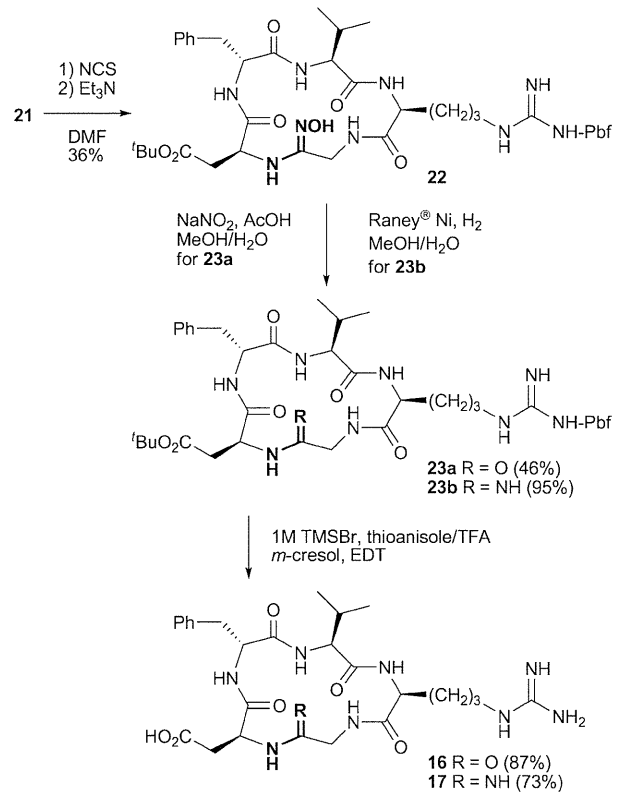

Scheme 4 Synthesis of cyclic RGD peptide **16** and amidine-type isosteric congener **17**.

Biological activity of the cyclic RGD Peptide with an amidine-type isosteric unit for the Gly-Asp dipeptide

The resulting cyclic RGD peptidomimetic **17** was evaluated for its inhibitory effect of integrin-mediated cell attachment (Fig. 2). Peptide **17**, with an amidine moiety, showed moderate inhibitory activity (IC_{50} = 4.77 μM) compared with original peptide **16** (peptide **16**, IC_{50} = 0.157 μM). The X-ray crystal structure of the $\alpha_v\beta_3$ integrin-cyclic RGD peptide complex indicated that the

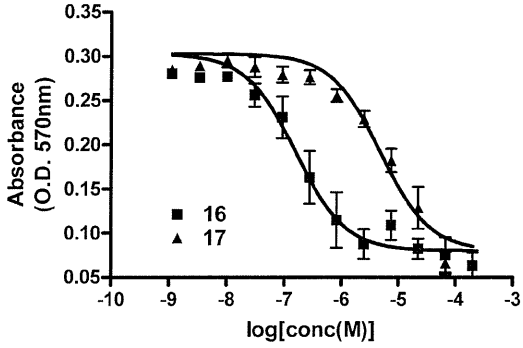

Fig. 2 The inhibitory effect of cyclic RGD peptides on HDF attachment to vitronectin. HDFs were allowed to attach to human vitronectin in the presence of various concentrations of cyclic RGD peptides. Peptides were added to the cell suspension and the cells were plated. After a 30 min incubation period, the attached cells were stained with crystal violet and dissolved in a 1% SDS solution. The absorbance at 570 nm was measured. Triplicate experiments gave similar results.

uncharged amide NH of Gly-Asp is located proximal to the integrin residue Arg216, which is likely to be involved in the interaction.[18] These results suggest that substitution of the Gly-Asp peptide bond with a positively-charged amidine unit partially eliminated the highly potent binding affinity towards the $\alpha_v\beta_3$ integrin.

Conclusion

In conclusion, we have established a novel approach to synthesize acyclic amidine and amide units *via* a key amidoxime (*N*-hydroxyamidine) precursor, which was prepared from a nitrile oxide component as an active ester equivalent. This method was used for the Fmoc-based solid-phase synthesis of peptides and peptidomimetics containing an amidine-type isostere. The peptide aldoxime represented a functional precursor for a protected cyclic peptide and peptidomimetic, suggesting that the nitrile oxide-mediated coupling reaction could serve as an alternative method for peptide macrocyclizations. Further studies on the scope and limitations of this approach, as well as applications for structure–activity relationship studies of bioactive peptides, are currently in progress.

Experimental section

Synthesis

***tert*-Butyl [(*S*)-1-(hydroxyiminomethyl)-2-methylpropyl]carbamate (9).** To a solution of Boc-Val-NMe(OMe) (5.00 g, 19.2 mmol) in Et_2O (60 cm^3) was added dropwise a solution of $LiAlH_4$ (1.02 g, 27.0 mmol) in Et_2O (20 cm^3) at –40 °C and the mixture was stirred for 40 min. The reaction was quenched at –40 °C by the addition of an Na_2SO_4 solution. The reaction mixture was washed with saturated aqueous $NaHCO_3$ and brine, and dried over Na_2SO_4. Concentration under reduced pressure gave the Boc-valinal. To a solution of $NH_2OH{\cdot}HCl$ (1.66 g, 23.9 mmol) and AcONa (1.96 g, 23.9 mmol) in EtOH (50 cm^3) was added the solution of the aldehyde in EtOH (15 cm^3). The reaction mixture was stirred at 80 °C for 15 min. The mixture was concentrated under reduced pressure. The residue was extracted with CH_2Cl_2, and the extract was washed with H_2O and dried over Na_2SO_4. Concentration under reduced pressure followed by flash chromatography over silica gel with n-hexane–EtOAc (3/1) gave the title compounds **9a** and **9b** (3.44 g, 82% yield, **9a**/**9b** = 58/42) both as white solids.

Compound **9a**: mp 35–36 °C; $[\alpha]_D^{26}$ +11.0 (*c* 0.58, $CHCl_3$); δ_H (500 MHz, DMSO, Me_4Si) 0.82 (6H, dd, *J* = 13.7 and 6.9 Hz), 1.37 (9H, s), 1.75 (1H, td, *J* = 13.7 and 6.9 Hz), 3.72–3.78 (1H, m), 6.96 (1H, d, *J* = 8.8 Hz), 7.14 (1H, d, *J* = 7.3 Hz) and 10.63 (1H, s); δ_C (125 MHz, DMSO-d_6, Me_4Si) 18.6, 18.8, 28.2 (3C), 30.9, 55.4, 77.7, 149.0 and 155.1. Anal. calc. for $C_{10}H_{20}N_2O_3$: C, 55.53; H, 9.32; N, 12.95. Found: C, 55.29; H, 9.17; N, 12.81%.

Compound **9b**: mp 114–115 °C; $[\alpha]_D^{26}$ +50.0 (*c* 0.18, $CHCl_3$); δ_H (500 MHz, DMSO-d_6, Me_4Si) 0.81 (6H, t, *J* = 7.2 Hz), 1.37 (9H, s), 1.76–1.85 (1H, m), 4.54 (1H, dd, *J* = 15.7 and 7.1 Hz), 6.51 (1H, d, *J* = 7.1 Hz), 6.95 (1H, d, *J* = 8.9 Hz) and 10.86 (1H, s); δ_C (125 MHz, DMSO, Me_4Si) 18.3, 18.7, 28.2 (3C), 30.7, 50.2, 77.7, 149.9 and 155.2. Anal. calc. for $C_{10}H_{20}N_2O_3$: C, 55.53; H, 9.32; N, 12.95. Found: C, 55.25; H, 9.32; N, 12.71%.

***tert*-Butyl (*S*)-2-{[(*S*)-2-*tert*-butoxycarbonylamino-*N*-hydroxy-3-methylbutanimidoyl]amino}-3-phenylpropionate (13).** To a solution of aldoxime **9b** (30.0 mg, 0.140 mmol) in DMF (0.6 cm^3) was added *N*-chlorosuccinimide (26.2 mg, 0.200 mmol) and the mixture stirred at room temperature for 4 h. The reaction mixture was extracted with EtOAc, the extract washed with a solution of H_2O/brine (1/1) and dried over Na_2SO_4. After concentration under reduced pressure, the residue was dissolved in Et_2O (5 cm^3). To the solution were added Et_3N (77 mm^3, 0.560 mmol) and H-Phe-O*t*Bu **12** (30.0 mg, 0.140 mmol), and the mixture stirred at room temperature overnight. The reaction mixture was washed with brine and dried over Na_2SO_4. Concentration under reduced pressure followed by flash chromatography over silica gel with n-hexane–EtOAc (3/1) gave title compound **13** (50.0 mg, 81% yield, inseparable mixture of major/minor = 97/3) as a colorless oil: $[\alpha]_D^{26}$ –19.2 (*c* 0.73, $CHCl_3$); δ_H (500 MHz, DMSO-d_6, Me_4Si) 0.63 (3H, d, *J* = 6.6 Hz), 0.73 (3H, d, *J* = 6.6 Hz), 1.32 (9H, s), 1.37 (9H, s), 1.79 (1H, dt, *J* = 21.7 and 6.6 Hz), 2.84–2.94 (2H, m), 3.70 (1H, t, *J* = 9.0 Hz), 4.44–4.52 (1H, m), 5.38 (1H, d, *J* = 10.5 Hz), 6.66 (1H, d, *J* = 9.5 Hz), 7.19–7.29 (5H, m) and 10.86 (1H, s); δ_C (125 MHz, DMSO-d_6, Me_4Si) 18.3, 19.8, 27.5 (3C), 28.2 (3C), 29.8, 55.0, 56.1, 77.8, 80.6, 126.5, 128.0 (3C), 129.5 (2C), 137.0, 150.5, 155.3 and 171.4; HRMS (FAB) *m*/*z* calc. for $C_{23}H_{38}N_3O_5$ ($[M + H]^+$) 436.2811, found 436.2808.

***tert*-Butyl (*S*)-2-{[(*S*)-2-*tert*-butoxycarbonylamino-3-methylbutanimidoyl]amino}-3-phenylpropionate (14).** To a solution of amidoxime **13** (29.1 mg, 0.0670 mmol) in MeOH (1 cm^3) and AcOH (0.011 cm^3) was added RANEY® Ni (0.85 cm^3, slurry in H_2O) and the mixture stirred under an atmosphere of hydrogen at room temperature for 1 h. The mixture was filtered through Celite®. Concentration under reduced pressure followed by flash chromatography over silica gel with n-hexane–EtOAc (3/1) gave title compound **14** (18.9 mg, 67% yield) as a yellow oil: $[\alpha]_D^{26}$ +7.53 (*c* 0.46, $CHCl_3$); δ_H (500 MHz, DMSO-d_6, Me_4Si) 0.76 (6H, dd, *J* = 13.5 and 6.7 Hz), 1.28 (9H, s), 1.38 (9H, s), 1.80–1.88 (1H, m), 2.86 (1H, br s), 2.92 (1H, dd, *J* = 13.5 and 6.9 Hz), 3.77 (1H, br s), 4.26 (1H, br s), 4.99 (1H, d, *J* = 9.5 Hz), 6.16 (1H, br s), 6.96 (1H, d, *J* = 9.5 Hz) and 7.14–7.26 (5H, m); δ_C (125 MHz, DMSO-d_6, Me_4Si) 18.0 (2C), 19.3, 27.5 (3C), 28.2 (3C), 31.0, 37.8, 59.5, 77.8,

78.9, 126.1, 127.9 (2C), 127.9, 129.2 (2C), 138.1, 155.2 and 171.2; HRMS (FAB) *m/z* calc. for $C_{23}H_{38}N_3O_4$ ([M + H]$^+$) 420.2862, found 420.2864.

***tert*-Butyl (*S*)-2-[(*S*)-2-*tert*-butoxycarbonylamino-3-methylbutyrylamino]-3-phenylpropionate (15).** To a solution of amidoxime **13** (35.3 mg, 0.0810 mmol) in MeOH (0.8 cm^3) and H_2O (0.8 cm^3) were added AcOH (0.00800 cm^3, 0.120 mmol) and $NaNO_2$ (8.30 mg, 0.120 mmol). The mixture was stirred at room temperature overnight. The mixture was concentrated under reduced pressure. The residue was extracted with CH_2Cl_2, and the extract was washed with H_2O and dried over Na_2SO_4. Concentration under reduced pressure followed by flash chromatography over silica gel with n-hexane–AcOEt (3/1) gave title compound **15** (21.0 mg, 62% yield) as a white solid: mp 115–116 °C; $[\alpha]_D^{24}$ +60.0 (*c* 0.87, $CHCl_3$); δ_H (500 MHz, DMSO-d_6, Me_4Si) 0.87 (3H, d, *J* = 5.6 Hz), 0.93 (3H, d, *J* = 6.8 Hz), 1.38 (9H, s), 1.45 (9H, s), 2.04–2.14 (1H, m), 3.04–3.11 (2H, m), 3.91 (1H, t, *J* = 6.8 Hz), 4.74 (1H, dd, *J* = 13.8 and 6.2 Hz), 5.16 (1H, d, *J* = 6.6 Hz), 6.30 (1H, d, *J* = 6.2 Hz) and 7.14–7.31 (5H, m); δ_C (125 MHz, DMSO-d_6, Me_4Si) 17.7, 19.2, 27.9 (3C), 28.3 (3C), 38.2, 52.2, 53.6, 55.1, 82.2, 82.3, 126.9, 127.0 (2C), 128.4 (2C), 129.5, 136.0, 170.3 and 171.0; HRMS (FAB) *m/z* calc. for $C_{23}H_{37}N_2O_5$ ([M + H]$^+$) 421.2702, found 421.2702.

H_2N–O-(2-Cl)Trt resin (18). 2-Chlorotrityl resin chloride (loading: 1.31 mmol g^{-1}, 76.3 mg) was reacted with Fmoc–NHOH (128 mg, 0.500 mmol) and pyridine (0.0810 cm^3, 1.00 mmol) in THF (0.8 cm^3) at 60 °C for 6 h. The solution was removed by decantation and the resulting resin washed with a solution of DMF/(^{i}Pr)$_2$NEt/MeOH (17/2/1). The Fmoc protecting group was removed by treating the resin with a DMF/piperidine solution (80/20, v/v). The loading was determined by measuring at 290 nm the UV absorption of the piperidine-treated sample: 0.900 mmol g^{-1}, 89%.

H–Asp(O^{t}Bu)–D-Phe–Val–Arg(Pbf)–Gly–aldoxime-(2-Cl)Trt resin (20). Solid-supported hydroxyamine **18** (loading: 0.900 mmol g^{-1}, 91.6 mg, 0.0820 mmol) was reacted with Fmoc-glycinal (0.500 mmol) in dichloroethane (0.7 cm^3), $HC(OMe)_3$ (0.5 cm^3) and AcOH (0.001 cm^3) at 60 °C for 2 h. The solution was removed by decantation and the resulting resin was washed with DMF to afford resin **19**. Peptide resin **20** was manually constructed using an Fmoc-based solid-phase synthesis on resin **19**. The Fmoc protecting group was removed by treating the resin with a DMF/piperidine solution (80/20, v/v). The Fmoc-protected amino acid (0.500 mmol, 6.1 equiv.) was successively condensed using 1,3-diisopropylcarbodiimide (0.0770 cm^3, 0.500 mmol, 6.1 equiv.) in the presence of *N*-hydroxybenzotriazole (77 mg, 0.500 mmol, 6.1 equiv.) to give resin **20**. The ^{t}Bu ester for Asp and 2,2,4,6,7-pentamethyldihydrobenzofuran-5-sulfonyl (Pbf) for Arg were employed for side-chain protection.

H–Asp(O^{t}Bu)–D-Phe–Val–Arg(Pbf)–Gly–aldoxime (21). Resin **20** was treated with TFA/TIS/CH_2Cl_2 (20 cm^3, 0.5/0.1/99.4) at room temperature for 1.5 h. After removal of the resin by filtration, the filtrate was concentrated under reduced pressure to give crude peptide aldoxime **21** as a yellow oil (74.0 mg, quant. from resin **18**). The crude product was used without further purification.

***Cyclo*[–Arg(Pbf)–Gly–ψ[C(=NOH)NH]–Asp(O^{t}Bu)–D-Phe–Val–] (22).** To a solution of peptide aldoxime **21** (74.0 mg) in DMF (1 cm^3) was added *N*-chlorosuccinimide (14.7 mg, 0.100 mmol). The solution was stirred at room temperature overnight, and then DMF (40 cm^3) and Et_3N (0.4 cm^3) added. The mixture was stirred at room temperature overnight and then concentrated under reduced pressure. The residue was extracted with EtOAc and the extract washed with brine. The organic layer was dried over Na_2SO_4 and concentrated under reduced pressure to give a yellow oil, which was purified by column chromatography over silica gel with CH_2Cl_2–MeOH (95/5) to give **22** (26.9 mg, 36% yield, major/minor = 79/21) as a yellow solid: mp 168–169 °C; $[\alpha]_D^{25}$ –52.7 (*c* 0.28, $CHCl_3$); δ_H (500 MHz, DMSO-d_6, Me_4Si) 0.85 (major, 3H, d, *J* = 6.9 Hz), 0.68 (minor, 3H, t, *J* = 6.4 Hz), 0.73 (major, 3H, d, *J* = 6.7 Hz), 0.72–0.76 (minor, 3H, m), 1.25–1.50 (2H, m), 1.34 (minor, 9H, s), 1.37 (major, 9H, s), 1.36 (minor, 6H, s), 1.41 (major, 6H, s), 1.74–1.76 (2H, m), 2.00 (3H, s), 2.41 (3H, s), 2.47 (3H, s), 2.30–2.50 (2H, m), 2.59 (1H, dd, *J* = 15.9 and 5.9 Hz), 2.82–2.91 (2H, m), 2.96 (2H, s), 3.79 (major, 1H, t, *J* = 7.0 Hz), 3.82–3.88 (minor, 1H, m), 3.98 (major, 1H, dd, *J* = 14.7 and 7.7 Hz), 4.02–4.08 (minor, 1H, m), 4.10–4.14 (minor, 1H, m), 4.16–4.25 (major, 1H, m), 4.50 (major, 1H, dd, *J* = 14.6 and 8.4 Hz), 4.35–4.45 (minor, 1H, m), 4.54–4.65 (major, 1H, m), 4.60–4.75 (minor, 1H, m), 5.17 (minor, 1H, d, *J* = 9.6 Hz), 5.27 (major, 1H, d, *J* = 10.6 Hz), 6.37 (major, 1H, br s), 6.70 (minor, 1H, br s), 7.12–7.33 (5H, m), 7.42–7.53 (1H, m), 8.05–8.14 (2H, m), 8.32 (minor, 1H, d, *J* = 7.3 Hz), 8.45 (major, 1H, d, *J* = 5.9 Hz), 9.17 (minor, 1H, s) and 9.63 (major, 1H, s); δ_C (125 MHz, DMSO-d_6, Me_4Si) 12.1, 12.3, 17.3 (minor), 17.6 (major), 17.8 (major, 2C), 17.9 (minor, 2C), 18.9, 19.0 (major), 19.1 (minor), 21.1, 27.7 (3C), 27.7, 28.3 (major, 2C), 28.8 (minor, 2C), 36.3, 42.5 (2C), 52.0, 52.6, 55.0, 59.8 (minor), 60.3 (major), 62.8, 79.7 (minor), 80.3 (major), 86.3, 116.3, 124.3, 126.5, 128.1 (minor, 2C), 128.2 (major, 2C), 129.1 (major, 2C), 129.3 (minor, 2C), 131.4, 134.2, 137.0, 137.3, 148.9, 156.0, 157.5, 169.3 (major), 169.5 (minor), 170.7, 171.2, 172.2 and 172.4; HRMS (FAB) *m/z* calc. for $C_{43}H_{64}N_9O_{10}S$ ([M + H]$^+$) 898.4497, found 898.4502.

***Cyclo*[–Arg(Pbf)–Gly–Asp(O^{t}Bu)–D-Phe–Val–] (23a).** To a solution of amidoxime **22** (20.0 mg, 0.0220 mmol) in MeOH (0.5 cm^3) and H_2O (0.2 cm^3) were added AcOH (0.00500 cm^3) and $NaNO_2$ (4.60 mg, 0.0660 mmol). The mixture was stirred at room temperature overnight. The mixture was concentrated under reduced pressure. The residue was extracted with EtOAc, and the extract washed with H_2O and dried over $MgSO_4$. Concentration under reduced pressure followed by PTLC purification with CH_2Cl_2–MeOH (95/5) gave title compound **23a** (8.90 mg, 46% yield) as a white solid: mp 247–248 °C; $[\alpha]_D^{25}$ –32.3 (*c* 0.27, MeOH); δ_H (500 MHz, DMSO-d_6, Me_4Si) 0.70 (6H, dd, *J* = 20.7 and 6.7 Hz), 1.18–1.50 (2H, m), 1.34 (9H, s), 1.41 (6H, s), 1.65–1.72 (1H, m), 1.80–1.88 (1H, m), 2.01 (3H, s), 2.36 (1H, dd, *J* = 15.7 and 8.9 Hz), 2.41 (3H, s), 2.46 (3H, s), 2.80 (1H, dd, *J* = 13.7 and 6.6 Hz), 2.91–3.06 (2H, m), 2.96 (2H, s), 3.28 (2H, s), 3.82 (1H, t, *J* = 7.6 Hz), 4.00–4.10 (2H, m), 4.54–4.62 (2H, m), 6.35 (1H, br s), 6.70–6.80 (1H, m), 7.13–7.28 (5H, m), 7.42–7.50 (5H, m), 7.74 (2H, dd, *J* = 11.5 and 8.3 Hz), 7.95 (1H, d, *J* = 8.3 Hz), 8.06 (1H, d, *J* = 7.6 Hz) and 8.36 (1H, dd, *J* = 7.3 and 4.4 Hz); δ_C (125 MHz, DMSO-d_6, Me_4Si) 12.3, 17.6, 18.2, 18.9, 19.2, 25.8, 27.6 (3C), 28.3 (2C), 28.4, 29.7, 36.4, 37.1, 39.8, 42.5, 43.1, 48.9,

52.2, 53.9, 60.1, 80.0, 86.3, 116.3, 119.7, 124.3, 126.2, 128.1 (2C), 129.0 (2C), 130.3, 131.4, 137.3, 156.0, 157.4, 169.1, 169.4, 169.9, 170.8, 171.0 and 171.1; HRMS (FAB) *m/z* calc. for $C_{43}H_{63}N_8O_{10}S$ ([M + H]$^+$) 883.4388, found 883.4397.

***Cyclo*[–Arg(Pbf)–Gly–ψ[C(=NH)NH]-Asp(O^{t}Bu)–D-Phe–Val–] (23b).** To a solution of amidoxime **22** (30.0 mg, 0.0330 mmol) in MeOH (0.6 cm^3) and AcOH (0.006 cm^3) was added RANEY® Ni (0.440 cm^3, slurry in H_2O), and the mixture stirred under a H_2 atmosphere at room temperature for 2 h. The mixture was filtered through Celite®. Concentration under reduced pressure followed by flash chromatography over silica gel with CH_2Cl_2–MeOH (95/5) gave title compound **23b** (27.4 mg, 95% yield) as a colorless oil: $[\alpha]_D^{26}$ –53.3 (*c* 0.14, $CHCl_3$); δ_H (500 MHz, CD_3OD, Me_4Si) 0.74 (6H, dd, *J* = 14.7 and 6.9 Hz), 1.43 (9H, s), 1.45 (6H, s), 1.45–1.52 (1H, m), 1.55–1.60 (1H, m), 1.82–1.89 (1H, m), 1.95–2.00 (1H, m), 2.07 (3H, s), 2.56 (3H, s), 2.59 (1H, d, *J* = 6.6 Hz), 2.77 (1H, dd, *J* = 16.5 and 6.9 Hz), 2.94 (1H, dd, *J* = 13.3 and 6.7 Hz), 2.99 (2H, s), 3.05 (1H, dd, *J* = 13.2 and 9.0 Hz), 3.11–3.18 (1H, m), 3.53 (1H, d, *J* = 15.2 Hz), 3.87 (1H, d, *J* = 6.9 Hz), 4.28 (1H, d, *J* = 15.2 Hz), 4.34–4.37 (1H, m), 4.39–4.45 (1H, m), 4.68 (1H, dd, *J* = 9.0 and 6.9 Hz) and 7.15–7.29 (5H, m); δ_C (125 MHz, CD_3OD, Me_4Si) 12.5, 18.4, 18.7, 19.6, 19.7, 28.4, 28.4, 28.4 (3C), 29.6 (2C), 30.9, 37.9, 38.4, 44.0, 49.5, 49.7, 54.0, 56.4, 62.5, 82.6, 87.7, 118.5, 126.0, 127.9, 129.6 (2C), 130.4 (2C), 132.4, 133.5, 134.4, 138.0, 139.4, 158.1, 160.0, 172.0, 173.3, 173.6, 173.9, 174.2 and 174.3; HRMS (FAB) *m/z* calc. for $C_{43}H_{62}N_9O_9S$ ([M – H]$^-$) 880.4397, found 880.4395.

***Cyclo*[–Arg–Gly–ψ[C(=NH)NH]–Asp–D-Phe–Val–] (17).** Protected amidine **23b** (7.90 mg, 0.00900 mmol) was treated with 1 M TMSBr–thioanisole in TFA (10 cm^3) in the presence of *m*-cresol (0.1 cm^3) and 1,2-ethanedithiol (0.5 cm^3) at 4 °C for 15 min. The mixture was poured into ice-cold dry Et_2O (50 cm^3). The resulting powder was collected by centrifugation and washed three times with ice-cold dry Et_2O. The crude product was purified by preparative HPLC to afford expected peptide **17** as a white powder (5.30 mg, 0.00660 mmol, 73% yield): $[\alpha]_D^{25}$ –129.2 (*c* 0.17, MeOH); δ_H (500 MHz, DMSO-d_6, Me_4Si) 0.70 (3H, d, *J* = 6.6 Hz), 0.74 (3H, d, *J* = 6.6 Hz), 1.32–1.60 (3H, m), 1.73–1.84 (1H, m), 1.88–1.98 (1H, m), 2.59 (1H, dd, *J* = 17.0 and 5.7 Hz), 2.78 (1H, dd, *J* = 13.5 and 6.5 Hz), 2.84 (1H, dd, *J* = 17.2 and 8.2 Hz), 3.00 (1H, dd, *J* = 13.0 and 8.4 Hz), 3.04–3.13 (2H, m), 3.72–3.78 (2H, m), 3.90–3.98 (1H, m), 4.23 (1H, dd, *J* = 13.5 and 8.2 Hz), 4.43 (1H, t, *J* = 16.2 and 7.0 Hz), 4.53–4.60 (1H, m), 4.62–4.68 (1H, m), 6.80–7.40 (2H, br s), 7.16–7.28 (5H, m), 7.72 (1H, t, *J* = 5.7 Hz), 7.93 (1H, dd, *J* = 11.3 and 8.4 Hz), 8.12 (1H, d, *J* = 7.7 Hz), 8.28–8.32 (1H, m), 8.53 (1H, d, *J* = 7.7 Hz), 8.92–8.98 (1H, m), 9.10–9.20 (1H, m) and 9.64 (1H, s); δ_C (125 MHz, DMSO-d_6, Me_4Si) 17.9, 25.3, 28.2, 29.6, 34.2, 37.0, 37.1, 40.2, 51.7, 51.9, 54.2, 59.9, 126.4, 128.2 (2C), 129.1 (2C), 137.2, 156.8, 158.4, 164.8, 166.8, 170.7, 171.2, 171.3 and 171.7; HRMS (FAB) *m/z* calc. for $C_{26}H_{40}N_9O_6$ ([M + H]$^+$) 574.3102, found 574.3101.

***Cyclo*(–Arg–Gly–Asp–D-Phe–Val–) (16).** By an identical procedure to that described for the preparation of **17**, **23a** (8.00 mg, 0.00900 mmol) was converted into cyclic RGD peptide **16** (0.00790 mmol, 87% yield). All characterization data were in agreement with the data for the control peptide, which was synthesized using Fmoc-based solid-phase synthesis. $[\alpha]_D^{25}$ –21.6 (*c* 0.27, MeOH); δ_H (500 MHz, DMSO-d_6, Me_4Si) 0.68 (3H, d, *J* = 6.7 Hz), 0.75 (3H, d, *J* = 6.7 Hz), 1.32–1.45 (2H, m), 1.45–1.55 (1H, m), 1.69–1.80 (1H, m), 1.80–1.90 (1H, m), 2.38 (1H, dd, *J* = 16.4 and 5.5 Hz), 2.72 (1H, dd, *J* = 16.4 and 8.9 Hz), 2.81 (1H, dd, *J* = 13.5 and 6.1 Hz), 2.94 (1H, dd, *J* = 13.5 and 8.0 Hz), 3.05–3.14 (2H, m), 3.26 (1H, dd, *J* = 15.2 and 4.2 Hz), 3.82 (1H, t, *J* = 7.4 Hz), 4.04 (1H, dd, *J* = 15.2 and 7.7 Hz), 4.08–4.16 (1H, m), 4.55 (1H, dd, *J* = 14.2 and 7.2 Hz), 4.60–4.68 (1H, m), 6.58–7.11 (1H, br s), 7.15–7.25 (5H, m), 7.58 (1H, t, *J* = 5.7 Hz), 7.78 (1H, d, *J* = 7.4 Hz), 7.87 (1H, d, *J* = 8.0 Hz), 8.00 (1H, d, *J* = 7.4 Hz), 8.08 (1H, d, *J* = 8.6 Hz), 8.36 (1H, dd, *J* = 7.4 and 4.2 Hz) and 12.3 (1H, s); δ_C (125 MHz, DMSO-d_6, Me_4Si) 18.1, 19.1, 25.3, 28.2, 29.5, 34.8, 37.1, 40.2, 43.0, 48.8, 52.0, 53.9, 60.1, 126.1, 128.0 (2C), 129.0 (2C), 137.3, 156.6, 158.3, 169.4, 169.8, 170.6, 171.1 and 171.6; HRMS (FAB) *m/z* calc. for $C_{26}H_{39}N_8O_7$ ([M + H]$^+$) 575.2942, found 575.2952.

Evaluation of inhibitory activity against integrin-mediated cell attachment. Human dermal fibroblasts (HDFs; AGC Techno Glass, Chiba, Japan) were maintained in DMEM containing 10% FBS, 100 U cm^{-3} penicillin and 100 μg cm^{-3} streptomycin (Invitrogen, Carlsbad, CA, USA). Human plasma vitronectin (0.1 μg in 0.050 cm^3 well^{-1}; EMD Chemicals Inc., Gibbstown, NJ, USA) were added to 96-well plates (Nalge Nunc, Rochester, NY, USA) and incubated for 1 h at 37 °C. The plates were washed and blocked with 1% bovine serum albumin (BSA; Sigma-Aldrich, St. Louis, MO, USA) in DMEM. HDFs were incubated at room temperature for 15 min in various concentrations of peptides (0.001–200 μM in 1% DMSO). Then, 0.100 cm^3 HDFs (2×10^4 cells) in DMEM containing 0.1% BSA were added to each well and incubated at 37 °C for 30 min in 5% CO_2. The attached cells were stained with a 0.2% crystal violet aqueous solution in 20% MeOH (0.150 cm^3) for 15 min. After washing with Milli-Q water, the plates were dried overnight at room temperature and dissolved in 0.150 cm^3 of a 1% SDS solution. The absorbance at 570 nm was measured. Each sample was assayed in triplicate, and cells attached to the BSA were subtracted from all measurements. 1% DMSO did not have any effect on HDF attachment to vitronectin.

Acknowledgements

This work was supported by Grants-in-Aid for Scientific Research and the Targeted Protein Research Program from the Ministry of Education, Culture, Sports, Science, and Technology of Japan. E. I. and K. T. are grateful for Research Fellowships from the JSPS for Young Scientists.

Notes and references

1 For reviews, see: (*a*) K. Burgess, *Acc. Chem. Res.*, 2001, **34**, 826; (*b*) M. G. Bursavich and D. H. Rich, *J. Med. Chem.*, 2002, **45**, 541; (*c*) V. J. Hruby, *J. Med. Chem.*, 2003, **46**, 4215.

2 (*a*) R. J. Abraham, S. L. R. Ellison, P. Schonholzer and W. A. Thomas, *Tetrahedron*, 1986, **42**, 2101; (*b*) T. E. Christos, A. Arvanitis, G. A. Cain, A. L. Johnson, R. S. Pottorf, S. W. Tam and W. K. Schmidt, *Bioorg. Med. Chem. Lett.*, 1993, **3**, 1035; (*c*) J. A. K. Howard, V. J. Hoy, D. O'Hagan and G. T. Smith, *Tetrahedron*, 1996, **52**, 12613; (*d*) J. Lin, P. J. Toscano and J. T. Welch, *Proc. Natl. Acad. Sci. U. S. A.*, 1998, **95**, 14020; (*e*) P. Wipf, T. C. Henninger and S. J. Geib, *J. Org. Chem.*, 1998, **63**, 6088.

Bioorganic & Medicinal Chemistry 19 (2011) 3216–3220

Contents lists available at ScienceDirect

Bioorganic & Medicinal Chemistry

journal homepage: www.elsevier.com/locate/bmc

Concise site-specific synthesis of DTPA–peptide conjugates: Application to imaging probes for the chemokine receptor CXCR4

Ryo Masuda, Shinya Oishi *, Hiroaki Ohno, Hiroyuki Kimura, Hideo Saji, Nobutaka Fujii *

Graduate School of Pharmaceutical Sciences, Kyoto University, Sakyo-ku, Kyoto 606-8501, Japan

ARTICLE INFO

Article history:
Received 17 February 2011
Revised 25 March 2011
Accepted 26 March 2011
Available online 2 April 2011

Keywords:
CXCR4
DTPA
Molecular imaging

ABSTRACT

Diethylenetriaminepentaacetic acid (DTPA) is a useful chelating agent for radionuclides such as ^{68}Ga, ^{99m}Tc and ^{111}In, which are applicable to nuclear medicine imaging. In this study, we established a facile synthetic protocol for the production of mono-DTPA-conjugated peptide probes. A novel monoreactive DTPA precursor reagent was synthesized in two steps using the chemistry of the *o*-nitrobenzenesulfonyl (Ns) protecting group, and under mild conditions this DTPA precursor was incorporated onto an N^{ε}-bromoacetylated Lys of a protected peptide resin. The site-specific DTPA conjugation was facilitated by using a highly acid-labile 4-methyltrityl (Mtt) protecting group for the target site of the bioactive peptide during the solid-phase synthesis. A combination of both techniques yielded peptides with disulfide bonds, such as octreotide and polyphemusin II-derived CXCR4 antagonists. DTPA–peptide conjugates were purified in a single step following cleavage from the resin and disulfide bond formation. This site-specific on-resin construction strategy was used for the design and synthesis of a novel In-DTPA-labeled CXCR4 antagonist, which exhibited highly potent inhibitory activity against SDF-1–CXCR4 binding.

1. Introduction

Recent progress in molecular imaging methodologies such as positron emission tomography (PET), single-photon emission computed tomography (SPECT) and optical imaging technologies has significantly improved the early detection and diagnosis of malignant tumors. To visualize the specific molecular events involved in the physiological and/or pathological processes, a number of peptide-based imaging probes have been developed for overexpressed receptors of peptide hormones and extracellular matrix proteins.[1] These probes are usually designed by a combination of three components: a target-specific vector peptide, an imaging part such as a radionuclide or fluorophore, and a linker to covalently or noncovalently conjugate the peptide with the imaging moiety. The addition of a functional moiety onto small-sized bioactive peptides may be highly susceptible to interaction with receptors or counterpart molecules. Consequently, there have been many reagents of choice for appropriate protein/peptide modifications. In addition, to determine the best labeling position from structure-function relationship studies, versatile synthetic approaches toward various types of labeled peptide are desired.

Polyamino polycarboxylate ligands efficiently coordinate metal radioisotopes to aid the radiolabeling of bioactive peptides. Among the chelating ligands, 1,4,7,10-tetraazacyclododecane-1,4,7,10-tetraacetic acid (DOTA) **1a** has been most widely utilized, since a variety of metal radioisotopes for both diagnostic and therapeutic purposes form complexes with high affinity and kinetic stability (Fig. 1).[2] DOTA-modification of bioactive peptides is facilitated by commercially available reagents such as DOTA-NHS **1b** and DOTA-maleimide **1c** to provide the expected peptides in a single step.[3,4] Alternatively, tris(*tert*-butyl)-DOTA **2a** with a free carboxyl group is employed for the modification of an amino group of protected peptides bound to solid-supports.[5] Lysine or phenylalanine derivatives **2b,c** possessing a *tert*-butyl-protected DOTA moiety are also useful components for the peptide sequence assembly.[6] *tert*-Butyl protecting groups in these reagents are easily removed during the final side-chain deprotection process of peptide synthesis.

In contrast to these DOTA derivatives, there has been limited work exploring the application of the diethylenetriaminepentaacetic acid (DTPA) chelating group **3a**, although DTPA represents a promising alternative, especially for ^{68}Ga, ^{99m}Tc and ^{111}In (Fig. 1). The recent success of DTPA-based probes is exemplified by a glucagon-like peptide-1 (GLP-1) receptor ligand, [Lys^{40}(Ahx-DTPA-^{111}In)NH_2]-exendin-4, for insulinoma diagnosis.[7] The DTPA group also works as a more favorable functional group than DOTA to facilitate the biological or biodistribution properties of several probes.[8] For the preparation of DTPA-conjugated imaging probes, several conjugation reagents have been developed. The most familiar cyclic diethylenetriaminepentaacetic dianhydride **4**

* Corresponding authors. Tel.: +81 75 753 4551; fax: +81 75 753 4570.
E-mail addresses: soishi@pharm.kyoto-u.ac.jp (S. Oishi), nfujii@pharm.kyoto-u.ac.jp (N. Fujii).

0968-0896/$ - see front matter © 2011 Elsevier Ltd. All rights reserved.
doi:10.1016/j.bmc.2011.03.059

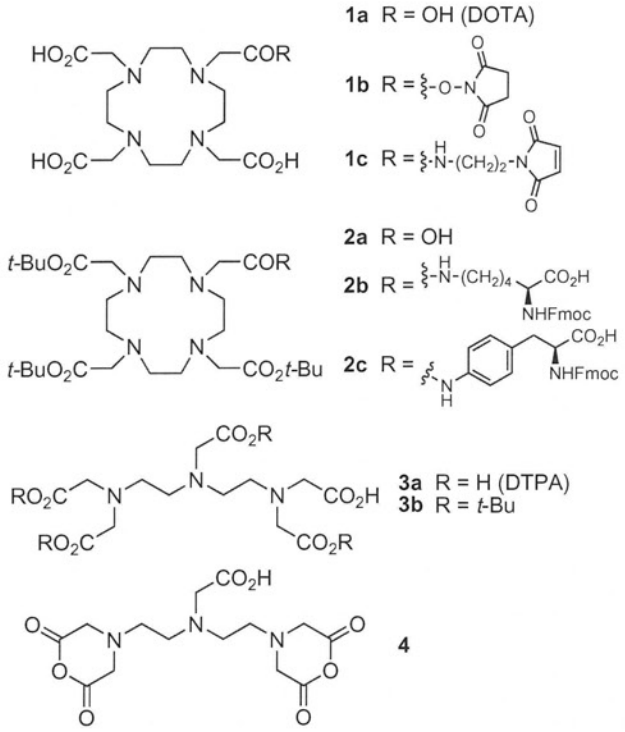

Figure 1. Structures of radionuclide chelating agents and the precursors.

is a bifunctional chelating agent, which can conjugate with peptide hormones and antibodies.[9] Using this reagent, concomitant formations of a bis-conjugated product[10] and intra- and intermolecular cross-linked products[11] were unavoidable. Monoreactive DTPA derivatives have also been developed for the preparation of DTPA–peptide conjugates without the unfavorable by-product formations.[12,13] For example, we reported the synthesis and application of 3,6,9,9-tetrakis[(*tert*-butoxycarbonyl)methyl]-3,6,9-triazanonanoic acid **3b** (mDTPA),[14] in which the four carboxylates were protected with *tert*-butyl ester. However, a longer process from the commercially available reagents is required for the synthesis of these DTPA-conjugation reagents (Scheme 1A).

Accordingly, to establish a facile and efficient synthetic method for DTPA–peptide conjugates, we have investigated the site-specific and on-resin construction of a DTPA moiety. Herein, we describe the short-step synthesis of a DTPA precursor using the *o*-nitrobenzenesulfonyl (Ns) protecting group and the solid-phase synthesis of DTPA–peptide conjugates. The design and synthesis of DTPA–peptide conjugates that potentially target the somatostatin receptor and chemokine receptor CXCR4 are also presented.[15]

2. Results and discussion

2.1. Synthesis of a DTPA-conjugation reagent and the application to octreotide derivatives

The synthetic scheme for the production of mDTPA reagent **10**, as described in our previous study, is presented in Scheme 1A. We hypothesized that two remedies could significantly improve the overall synthetic process of DTPA–peptide conjugates. First, the use of an Ns group in place of the trifluoroacetyl group was expected to serve as a temporary protecting group and an auxiliary group for global modification with four *tert*-butoxycarbonylmethyl groups. This potentially improves the stepwise synthesis of the intermediate **7** in the solution-phase. In addition, a secondary amine **8** as a nucleophilic precursor for the bromoacetyl group on peptide resin **11** can directly produce the overall DTPA framework of **12** on the solid support without the additional three-step modification process of **8** in solution (Scheme 1B).[16]

Synthesis of DTPA precursor **8** began with mono-Ns protection of the commercially available diethylenetriamine **5** (Scheme 2). The Ns-protected intermediate was successively treated with excess equivalent of *t*-butyl bromoacetate in a one-pot process. Although the solvent EtOH has been reported to be effective in predominantly giving the mono-Ns product,[17] concomitant production of bis-Ns product **14b** was not suppressed as in DMF. The treatment of excess diethylenetriamine **5** with NsCl in EtOH provided mono-Ns product **14a** in 65% yield (calculated based on NsCl), which can be readily purified by chromatography. Compound **14a** was then subjected to deprotection with mercaptoacetic acid and LiOH to provide the expected precursor **8** in 77% yield.

Using the resulting reagent **8**, DTPA-conjugation of [D-Phe^1]octreotide was investigated as a model study (Scheme 3), which is employed as a radionuclide imaging probe for the somatostatin receptor.[14,18,19] After peptide-chain elongation by Fmoc-based solid-phase peptide synthesis, the N-terminus of **16** was modified with bromoacetic acid and 1,3-diisopropylcarbodiimide (DIC). Subsequently, the bromide **17** was treated with the reagent **8** in the presence of $(i\text{-Pr})_2$NEt to provide the fully protected peptide resin **18a**. Cleavage from the resin **18a** and disulfide formation under air-oxidation conditions provided [DTPA-D-Phe^1]octreotide **19a** with high purity. The bromoacetylated peptide **17** was also modified with commercially available DOTA precursor reagent **20**, using the identical procedure to provide [DOTA-D-Phe^1]octreotide **19b**.[20] These suggest that this on-resin modification procedure is widely applicable to any chelating reagents with nucleophilic functional groups such as DTPA and DOTA precursors.

2.2. Site-specific DTPA-conjugation of bioactive peptides: synthesis of CXCR4 receptor probes

It has been reported that a high level of CXCR4 expression in tumors is associated with malignant and metastatic properties.[21] Intrinsic SDF-1 release from the potential distal metastatic sites mediates organ-specific metastasis of CXCR4-expressing cells from the primary lesions. Since CXCR4-expressing cancer stem cells are related to the metastatic spread in orthotopic primary tumors,[22] it is of considerable importance to develop potent CXCR4-imaging probes to detect potential cancer stem cells within malignant tumors, as exemplified by the diagnosis of bladder cancer by a fluorescent CXCR4 probe.[23,24]

Previously, we reported a DTPA-conjugated CXCR4 antagonist, DTPA-Ac-TZ14011 **26a**,[25] which was designed from a horseshoe crab-derived anti-HIV peptide T140. This peptide has β-sheet-like structures maintained by a disulfide bond, around which the pharmacophore residues for bioactivity are located.[26] For the site-specific conjugation at D-Lys^8 in the type II' β-turn region of T140 with a single DTPA group in the solution-phase, a secondary lysine (Lys^7) was substituted with arginine, which cannot be acylated by standard reagents.[25] Although a DTPA group was successfully ligated with maintenance of highly potent CXCR4 antagonistic activity in this case,[25] the accompanying substitutions needed for specific modification of other peptides may possibly lead to a decrease in the bioactivity. Therefore, we planned the facile site-specific DTPA conjugation on a solid-support for production of CXCR4 imaging probes without substitution of the secondary Lys^7 residue. To distinguish D-Lys^8 to be labeled in peptides **26**, the highly acid-labile 4-methyltrityl (Mtt) group was exploited for temporary protection of the ε-amino group during solid-phase peptide synthesis.[27] For the other Lys residues such as Lys^7 of